

**Acoustoelasticity in 7075-T651 Aluminum and Dependence
of Third Order Elastic Constants on Fatigue Damage**

A Thesis
Presented to
The Academic Faculty

by

David M. Stobbe

In Partial Fulfillment
of the Requirements for the Degree
Masters of Science

School of Mechanical Engineering
Georgia Institute of Technology
August 2005

Acoustoelasticity in 7075-T651 Aluminum and Dependence of Third Order Elastic Constants on Fatigue Damage

Approved by:

Professor Thomas E. Michaels, Adviser
School of Mechanical Engineering
Georgia Institute of Technology

Professor Jianmin Qu
School of Mechanical Engineering
Georgia Institute of Technology

Professor Laurence J. Jacobs
School of Civil Engineering
Georgia Institute of Technology

Date Approved: July 11, 2005

ACKNOWLEDGEMENTS

First, I would like to thank my advisor Dr. Thomas Michaels for his guidance and patience. I thank Dr. Michaels for his patience with my brazenness while still embracing and fueling my enthusiasm. From common sense adages to complex mathematics Dr. Michaels has provided a cornucopia of knowledge.

I would also like to thank my committee and research professors Dr. Jennifer Michaels, Dr. Jianmin Qu, Dr. Laurence Jacobs, Dr. Jin-Yeon Kim, and Dr. Bao Mi. All of you have always been more than willing to help me with my own research, when in fact it is I who was hired to help you with your research. I hope that I have taught or helped you even 1/100 of what you have done for me.

I would like to thank my research lab colleagues Adam Cobb, Bo Marr, Yinghui Lu, and Dr. Bao Mi. All of you put up with so much of my lab hijinks, that you each deserve a field medal. Between my constant complaining, equipment monopolies, and lab filling messiness, it's a wonder any of you got anything done. So, thanks for putting up with me.

I would like to make a special thanks to Adam Cobb and Dr. Bao Mi. The three of us spend many many hours toiling away in the highbay working on the DARPA project, and I haven't forgotten a single minute of it. As the Michaels first graduate team, I like to think that the three of us had a unique experience together, and while I'm sad to see it end, I'm sure glad it's over. I hope the two of you learned as much from me as I did from you, and I'm not just talking about engineering.

I'd also like to thank my friends and family. I'd like to thank my family for providing me with this opportunity and for always supporting my decisions. I'd like to thank my friends for tolerating my incessant whining about how tough my life is. No matter how boring I became, after months of writing, you were all there to attentively listen about how horrible it was, thanks.

Finally, I'd like to thank the Defense Advanced Research Projects Agency (DARPA).

It was only through your continual commitment to the advancements of science and engineering that I was able to attend graduate school. I hope that some of the research I have performed here at Georgia Institute of Technology will be put to good use.

TABLE OF CONTENTS

ACKNOWLEDGEMENTS	iii
LIST OF TABLES	vii
LIST OF FIGURES	ix
SUMMARY	xii
I INTRODUCTION AND LITERATURE REVIEW	1
1.1 Introduction and History of Acoustoelasticity	1
1.2 Physical Theory, Mathematics, and Modeling	3
1.2.1 Physics of Material Nonlinearity: Acoustoelasticity and The Third Order Elastic Constants	3
1.2.2 Derivation of Third Order Elastic Constants	7
1.2.3 Other Sources of Nonlinearity	10
1.2.4 2-D Reflection and Refraction Model	11
II EXPERIMENTATION	17
2.1 Aluminum Specimens, Fatiguing, and Ultrasonic Equipment	17
2.1.1 Sample Description	17
2.1.2 Fatiguing	19
2.1.3 Ultrasonic Testing Equipment	21
2.2 Immersion Testing: Experimental Setup for Longitudinal Acoustoelastic Constants and Strain Mapping	22
2.2.1 Experimental Setup	23
2.2.2 Tooling and Techniques Aimed at Reducing Geometric Errors	26
2.3 Longitudinal Acoustoelastic Constants and Strain Mapping	32
2.3.1 Longitudinal Acoustoelastic Constants	32
2.3.2 Strain Mapping	35
2.4 Contact Transducer Testing: Shear Acoustoelastic Constants	36
2.4.1 Contact Testing: Experimental Setup	36
2.4.2 Shear Acoustoelastic Constants	38

III DATA ANALYSIS AND SIGNAL PROCESSING	41
3.1 Immersion Testing: Longitudinal Acoustoelastic Constants and Strain Mapping	41
3.1.1 Longitudinal Acoustoelastic Constants: TOF and Thickness	41
3.1.2 Strain Mapping	44
3.2 Contact Testing: Shear Acoustoelastic Constants	44
3.2.1 Shear Acoustoelastic Constants: TOF and Thickness	46
IV RESULTS AND CONCLUSION	48
4.1 Decomposing the Acoustoelastic Constant: Density Effect and Elastic Non-linearity	48
4.2 Longitudinal Testing: Results and Conclusions	53
4.2.1 Longitudinal Acoustoelastic Constant Results	53
4.2.2 Strain Mapping Results	57
4.3 Results for Contacting Testing: Shear Acoustoelastic Constants	60
4.4 Third Order Elastic Constants For 7075-T651 Aluminum and Their Variation with Damage	64
4.5 Uncertainty and Error Propagation	68
V APPLICATION OF TOEC	71
VI CONCLUSIONS AND RECOMMENDATIONS	74
APPENDIX A — CHANGE IN ELASTICITY AS A FUNCTION OF STRAIN	76
REFERENCES	78

LIST OF TABLES

1	Table containing the longitudinal and shear acoustic wave velocities for aluminum and water at 20 C°	14
2	Table containing the densities for aluminum and water at 20 C°	15
3	Table of mechanical properties for 7075-T6 aluminum	17
4	Table listing the important settings for the Panametrics 5900 Pulser Receiver.	33
5	Table listing the important acquisition settings for the Scan View Plus software.	33
6	Table listing the fatigue damage of each sample.	35
7	Table showing contribution of the density effect on the acoustoelastic constant at a static stress of 350 MPa for each case investigated.	51
8	Table showing the elastic nonlinearity effect on the acoustoelastic constant and percent change in Young's modulus at a uniaxial static stress of 350 MPa for each case investigated	52
9	Table showing acoustoelastic constant for a longitudinal wave traveling perpendicular uniaxial stress. Values from this paper are shown and the values from several other sources whom have performed similar tests.	55
10	Table showing acoustoelastic constant for a longitudinal wave traveling perpendicular a uniaxial stress. Values are shown for undamaged and damaged samples.	56
11	Table showing the experimental value for Young's modulus.	59
12	Table comparing strain as a function of stress at various locations along the gauge section.	60
13	Table comparing strain as a function of stress for each sample.	60
14	Table showing acoustoelastic constant for a shear wave traveling perpendicular a uniaxial stress with particle motion perpendicular uniaxial stress. Values from this paper are shown and the values from several other sources whom have performed similar tests.	61
15	Table showing acoustoelastic constant for a shear wave traveling perpendicular a uniaxial stress with particle motion parallel uniaxial stress. Values from this paper are shown for undamaged and damaged samples as well as the values from several other sources whom have performed similar tests.	63
16	Table showing the change in the acoustoelastic constant for shear waves with damage. This table shows the percent change for shear waves of opposite polarization.	64
17	Table showing how the acoustoelastic constant changes during fatigue life for a shear wave polarized with particle motion parallel an applied uniaxial stress.	64

18	Table listing the second and third order elastic constants for 7075-T651 aluminium.	66
19	Table listing the third order elastic constants for 7075-T651 aluminium versus damage.	67
20	Strain uncertainty propagation through the calculation of a shear wave acoustoelastic constant.	69
21	Strain uncertainty propagation through the calculation of a longitudinal wave acoustoelastic constant.	70
22	Table detailing the change in Young's modulus with applied stress for shear waves traveling perpendicular a uniaxial stress polarized parallel and perpendicular to an applied uniaxial stress.	77

LIST OF FIGURES

1	Typical binding energy as a function of atomic spacing for covalent bonding.	6
2	Typical binding force as a function of atomic spacing for covalent bonding.	6
3	Force as a function of atomic spacing zoomed near the inter-atomic equilibrium separation. Moving away from equilibrium shows how the elasticity is effect by lattice strain.	7
4	Stress strain relationship for a crystal orientation relative to a uniaxial loading.	11
5	Two dimensional diagram showing the reflections and refractions of a plane wave normal incident on multiple interfaces of water and aluminum. The signals of interest are labeled and the recorded pulses are stated.	13
6	Ultrasonic signal recorded from the geometric setup in Fig. 5 where the two pulses correspond to the stated wave paths.	13
7	Two dimensional diagram showing the reflections and refractions of a plane wave at an incident angle on a water aluminum interface.	15
8	Engineering drawing for dog-bone samples used. Drawing contains dimensions in inches and mili-meters.	17
9	Optical image of sample microstructure. Image shows a plane perpendicular to the cold rolling direction	18
10	Optical image of sample microstructure. Image shows a plane parallel to the cold rolling direction	18
11	A portion of the fatigue loading spectrum used to damage samples.	19
12	Average stress and strain of a sample during fatiguing.	20
13	Diagram outlining the setup for generating and recoding ultrasonic waves.	22
14	Picture showing the yoke attachment for the scanning head, immersion transducers, and search tubes.	23
15	Section drawing of the static loading fixture with key components labeled.	24
16	Diagram showing the geometry of the yoke, transducers, and sample. Two positions of the yoke are shown and important lengths are labeled.	24
17	Picture of the static loading fixture in the immersion take with scanning arm in data acquisition position	25
18	Diagram of the error produced when the transducer beam is not normal to the sample face.	27
19	Waveform energy as a function of swivel angle. The energy data is curve fit in order to determine the angle at which the maximum energy is reflected to the receiver.	28

20	Diagram of the sample movement due to loading off centroid.	28
21	Section view of leveling fixture. Drawing details the samples position relative to the fixture and where the four contact points of the leveling fixture are located.	29
22	Assembly drawing for the leveling fixture showing the various components and how they are jointed.	30
23	Zoomed section drawing showing the housing pieces used for the linear thread differential and the leveling rods.	30
24	Picture of a sample face being leveled with the dial indicator and flat bar tooling.	31
25	Simplified model of the angle errors in swivel and gimbal due to non normal transducer beam to sample surface.	32
26	Drawing detailing the dimensions of the three specific locations, along the gauge section, where the ultrasonic measurements are taken. These positions are shown in relation to the side of the sample which the load is applied and the side that is anchored.	33
27	Ultrasonic waveform for a signal transmitted from one transducer to the adjacent transducer in the yoke, the only medium traversed is water 20°C. .	34
28	Ultrasonic waveform for a pulse echoed transducer. The first pulse is the water path reflection only. The second pulse is reflected off the back wall of the sample.	34
29	Ultrasonic waveform for a pulse echoed transducer. The pulse is the water path reflection off the front wall of the sample.	35
30	Schematic of shear wave transducer showing how orientation controls the wave polarization (particle motion) relative to the applied load direction. .	37
31	Pictures of shear wave transducer orientated with the polarization such that the particle motion is perpendicular or parallel to the loading direction. . .	37
32	Schematic detailing the wave paths for the two ultrasonic pulses recorded. .	38
33	Picture of C-clamp mounting the shear transducer to a sample.	39
34	Plot showing three time of flight versus loading data sequences. The data sets show the effect of removing and rebonding the transducer.	39
35	Ultrasonic waveform for a pulse echoed shear transducer. The first pulse is the reflection off the couplant front wall interface. The second pulse is the reflection from the back wall of the sample.	40
36	Plot showing typical immersion testing experimental data of sample thickness as a function of uniaxial load.	42
37	Plot showing typical immersion testing experimental data of time of flight as a function of uniaxial load.	43

38	Plot showing typical immersion testing experimental data of longitudinal wave velocity as a function of uniaxial load.	44
39	Plot showing typical immersion testing experimental data of longitudinal wave velocity as a function of uniaxial stress.	45
40	Plot showing typical immersion testing experimental data of sample strain as a function of applied uniaxial stress.	45
41	Plot showing typical shear testing experimental data of time of flight as a function of uniaxial load.	46
42	Plot showing typical shear testing experimental data of longitudinal wave velocity as a function of uniaxial stress.	47
43	Acoustoelastic constant for each undamaged sample. Acoustoelastic constant is for longitudinal waves traveling perpendicular to applied uniaxial stress with particle motion perpendicular to applied uniaxial stress.	53
44	Acoustoelastic constant for three positions along the gauge section of undamaged samples. Acoustoelastic constant is for longitudinal waves traveling perpendicular to applied uniaxial stress with particle motion perpendicular to applied uniaxial stress.	54
45	Acoustoelastic constant for undamaged and damaged samples. Acoustoelastic constant is for longitudinal waves traveling perpendicular to applied uniaxial stress with particle motion perpendicular to applied uniaxial stress.	56
46	Plot of all immersion testing experimental data for transverse strain versus stress. Symbols corresponding to each sample.	58
47	Plot of all immersion testing experimental data for transverse strain versus stress. Symbols corresponding to each position along gauge section.	59
48	Acoustoelastic constant for undamaged and damaged samples. Acoustoelastic constant is for shear waves traveling perpendicular to applied uniaxial stress with particle motion perpendicular to applied uniaxial stress.	61
49	Acoustoelastic constant for undamaged and damaged samples. Acoustoelastic constant is for shear waves traveling perpendicular to applied uniaxial stress with particle motion parallel to applied uniaxial stress.	62
50	Third order elastic constants for undamaged and damaged samples.	67
51	Shear transducer setup for third order elastic constant application problem.	71
52	Waveform showing the two pulses representing the single and double V wave paths and TOF shift with applied static loading [17].	72
53	Experimental TOF data versus theoretical TOF [17].	73

SUMMARY

Acoustoelasticity is the stress dependence of acoustic wave velocity in elastic media. This effect is a manifestation of the inherent nonlinearity in the stress strain constitutive relation and the variation in density under elastic deformation. This paper explores the acoustoelastic effect in rolled 7075-T651 aluminum.

The acoustoelastic effect is explored using acoustoelastic constants and third order elastic constants. These parameters, describing material nonlinearity, are calculated and mapped versus fatigue damage. Mathematics and physics modeling are used to describe acoustoelasticity and justify fatigue mapping.

The acoustoelastic effect for three ultrasonic waves are measured and explored. The three waves are a longitudinal wave traveling normal to an applied uniaxial stress, a shear wave traveling normal to an applied uniaxial stress with particle motion normal stress, and a shear wave traveling normal to an applied uniaxial stress with particle motion parallel stress.

Ultrasonic techniques for determining the acoustoelastic constants are presented. Immersion testing and contact testing are the primary ultrasonic techniques used. These techniques are detailed in terms of setup, signal processing, and experimental errors.

Results for the acoustoelastic constants and third order elastic constants experimentation is presented. These results include the numerical value of the acoustoelastic constants and the third order elastic constants as well as their dependence on fatigue damage.

The results show that there is a trend in acoustoelasticity with fatigue damage. This trend is most apparent in the acoustoelastic constant for a shear wave traveling normal to an applied uniaxial stress with particle motion parallel stress. There is a trend in the third order elastic constants with fatigue damage. Further, an application of the third order elastic constants in a separate research project is shown, and corroborates the experimental values.

CHAPTER I

INTRODUCTION AND LITERATURE REVIEW

1.1 Introduction and History of Acoustoelasticity

Acoustoelasticity is the stress dependence of acoustic wave velocity in elastic media. The acoustoelastic effect has been studied for over 40 years, for a variety of purposes.

The modern theory of acoustoelasticity was developed in the 1950s by Hughes and Kelly [13]. They were interested in calculating the third order elastic constants (TOEC) in crystals. Using third order energy terms in their constitutive equations and Murnaghan's theory of finite displacements, Hughes and Kelly determined that for isotropic materials, in addition to the two Lamé constants, λ and μ , three additional constants, l , m , and n , are required to describe a material. These constants can be determined by measuring the change in acoustic phase velocity as a function of stress. Hughes and Kelly experimentally determined the TOEC of polystyrene, iron, and Pyrex glass. Their mathematical derivation of the TOEC is shown in Section 1.2.2.

Acoustoelastic theory for hyperelastic materials of arbitrary symmetry was developed in 1961 by Toupin and Berstein [21]. This theory was expanded and revised by Thurston and Brugger in 1963 using the concept of *natural velocities*, which use a superposition of perturbations over a natural state [20]. Exact acoustic velocity formulas were derived for arbitrary crystal symmetry and arbitrary stress systems using the second and third order elastic constants of a material. However, application of these formulations to real systems is cumbersome and impractical except for the case of hydrostatic pressure and uniaxial stress of cubic point groups and isotropic materials.

Acoustoelasticity was used to predict applied stresses in its first application ([7][12][15][4]). Engineers in the late 1950's and early 1960's attempted to use acoustoelasticity as a non-destructive means for evaluating a system's stress state, the first being Bergman and Shahbender in 1958 and Benson and Raelson in 1959.

This early application of acoustoelastics was riddled with uncertainty and inconsistency. The primary inadequacy, besides equipment resolution, was an inconsistent material state. TOEC measurements would vary depending on the material processing, such as casting, rolling, or drawing. This dependence on processing was traced to the presence of residual, or internal, stresses. The degree, depth, and location of residual stresses influences the acoustoelastic properties. In leu of this discovery, engineers began using acoustoelastics to not only measured applied stresses, but residual stress as well ([19][16][10][5][8][6]).

The most current research thrust, in terms of acoustoelastics, has been the measuring of residual stress. Three major difficulties are hindering the advancement of this technology.

First, the acoustoelastic effect is small, typically of the order 0.001% per MPa of applied stress, for metals. This minutia dictates strict precision in experimentation. This complication is becoming less of an issue with the advent of high performance microprocessors and powerful discretizing hardware.

Second, the inherent or induced preferred orientation of crystalline grains effects acoustoelasticity. This orientation, called texture, causes an anisotropic effect in the material properties. This anisotropic effect has been compensated for by theoretical revisions in acoustoelastic theory or special experimental techniques, such as the Generalized Acoustic Ratio (GAR) technique [8].

The third major problem is the unknown influence of localized plastic deformation. This problem is also caused by material processing and is closely related to residual stresses. Residual stresses are a manifestation of local plastic deformation. The plastically deformed lattices will not have the same acoustoelastic properties as the elastic lattices and hence must be accommodated for. Unfortunately, little to no research as been done to determine the “acousto-plastic” relationship.

This paper, however, is not concerned with furthering the specifics of acoustoelastic theory or experimentation, in terms of accurately measuring residual or applied stress. Rather, this paper will present several ultrasonic techniques for measuring acoustoelasticity, report specific values for several acoustoelastic constants of rolled bar 7075-T651 aluminum, and map the acoustoelastic constants with fatigue damage. Using these acoustoelastic

constants the TOEC for 7075-T651 aluminum are also determined. Further, the relative values for the acoustoelastic constants, defined by the acoustic wave particle motion and propagation direction relative to applied stress, are studied and explained using mathematics and physics modeling. The experimentation used to determine acoustoelasticity also lent itself to an investigation of ultrasonic strain mapping.

1.2 Physical Theory, Mathematics, and Modeling

The following section will explore the physics behind acoustoelasticity, the rigorous mathematics of the third order elastic constants, and some simple models of wave reflection and refraction. The physics section will show how the nonlinearity in the inter atomic binding energy gives rise to strain depend second order elastic constants. Then the mathematics, borrowed from Hughes and Kelly, will detail how including third order elastic terms can compensate for material nonlinearity. And finally, the modeling section will show how a stress wave's amplitude, polarization, and direction of propagation is changed at an interface of two elastic half spaces.

1.2.1 Physics of Material Nonlinearity: Acoustoelasticity and The Third Order Elastic Constants

Acoustoelasticity refers to the dependence of ultrasonic wave velocity on applied stress. This phenomenon occurs in concordance with continuum theory of small disturbances superimposed on elastically deformed bodies [18]. Acoustic phase velocity, in solids, is dependent on the material's mass and elastic properties. For example, the longitudinal wave velocity in a thin rod is, Eq. 1,

$$C_L = \sqrt{\frac{E}{\rho}} \quad (1)$$

where E and ρ are Young's modulus of elasticity and density, respectively. A body's density and elasticity will change under stress, thus causing a variation in the acoustic velocity.

The density variation with stress is easily seen using Hooke's law in three dimensions, Eq. 2, where σ and ϵ are the stress and strain, respectively. A simple case is a cube of an

isotropic material under uniaxial stress.

$$\begin{aligned}\sigma_x &= \frac{1}{E}[\epsilon_x - \nu(\epsilon_y + \epsilon_z)] \\ \sigma_y &= \frac{1}{E}[\epsilon_y - \nu(\epsilon_x + \epsilon_z)] \\ \sigma_z &= \frac{1}{E}[\epsilon_z - \nu(\epsilon_x + \epsilon_y)]\end{aligned}\tag{2}$$

If the cube is strained one unit in the direction of loading, the opposing two sides will contract by ν , Poisson's ratio, where $\nu < 0.5$ [9]. The net volume will increase proportional to $1 - 2\nu$, the mass is conserved, thus yielding a net decrease in material density with elastic loading. This term is called the density effect. A more formal derivation of this effect and it's contribution to acoustoelasticity is explored in Section 4.1.

The elastic variation under stress arises from the nonlinearity of the stress strain relationship. Mathematically this nonlinearity appears as the higher order terms in the Taylor series expansion of the constitutive law and is shown in indicial notation in Eq. 3, where U is the strain energy and the C 's are elastic tensors of different degree.

$$\begin{aligned}\sigma_{ij} &= \frac{\partial U}{\partial \epsilon_{ij}} \\ U &= C^{(0)} + C_{ij}^{(1)} \epsilon_{ij} + \frac{1}{2} C_{ijkl}^{(2)} \epsilon_{ij} \epsilon_{kl} + \frac{1}{6} C_{ijklmn}^{(3)} \epsilon_{ij} \epsilon_{kl} \epsilon_{mn} \dots\end{aligned}\tag{3}$$

The nonlinear terms are often neglected, as they are small and make the mathematics much more difficult. However, for acoustoelasticity the higher order terms are retained and are in fact the parameters of interest. The strict mathematics of the higher order elastic tensor will be shown in detail in the next section. For now let us explore the physics behind the TOEC, as the insight will give meaning to load directional dependencies and fatigue mapping.

In order to understand the origin of the TOEC, and all other higher order nonlinear components of the stress strain relationship, we will consider the covalent bonds of an isotropic crystalline metal.

The interatomic bond of two ions can be described with a sum of two energy terms, an attractive and a repulsive. The attractive energy is driven by the electrostatic force and for

ionic bonding is described by Eq. 4 [2],

$$U_a = \frac{q^2}{4\pi\epsilon_o r} \quad (4)$$

where r , q , and ϵ_o are the interatomic spacing, fundamental charge, and permittivity in a vacuum, respectively, and is seen for covalent bonding in Fig. 1. The repulsive energy is caused by the repulsion of the two nuclei and for ionic bonding is described by Eq. 5 [2],

$$U_r = \frac{q^2 r_o^{n-1}}{4\pi\epsilon_o n r^n} \quad (5)$$

where n is large power, typically 12, and r_o is the equilibrium atomic bond length, and is seen for covalent bonding in Fig. 1. “A covalent material presents a difficult challenge because complex quantum-mechanical effects such as chemical bond formation and rupture, hybridization, metallization, charge transfer and bond bending must be described by an effective interaction between atoms in which the electron degrees of freedom have somehow been integrated out” [3]. However, the energy of a covalent bond is well described by the empirical relationship in Eq. 6,

$$U = -\frac{A}{r^m} + \frac{B}{r^n} \quad (6)$$

where $m < n$ and A and B are constants [2].

Figure 1 is a heuristic model using Eq. 6 with values of m , n , A , and B typical of metallic bonding [2]. Using the energy curve, the force for any atomic separation can be found by differentiation of Eq. 6 (Fig. 2).

In Fig. 2, the net curve shows the interatomic force caused by straining the lattice. The slope of this curve is a measure of the elasticity of a metal,

$$E = \frac{1}{r_o} \left(\frac{\partial^2 U}{\partial r^2} \right)_{r=r_o} \quad (7)$$

where E is Young’s modulus and U is the total energy [2]. In fact, a “pure value” for Young’s modulus of elasticity can be calculated this way. However, these specific values are highly idealized and thus rather unimportant. What is important is how the elasticity changes with strain.

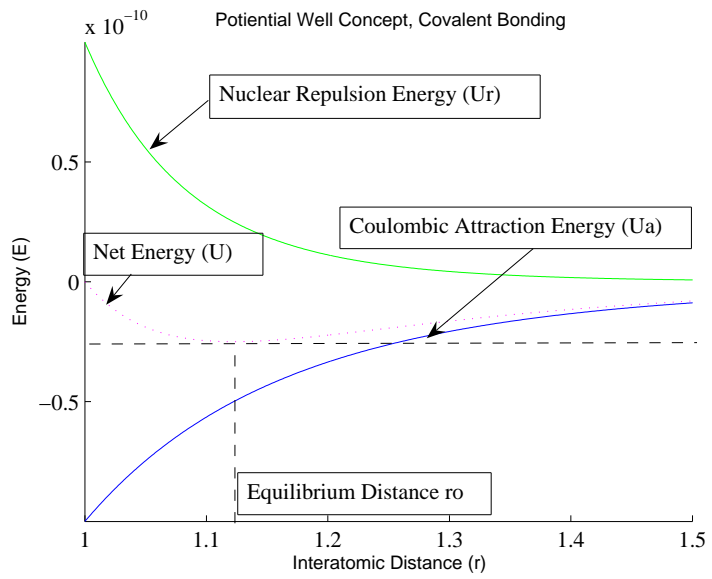


Figure 1: Potential Energy Well for Covalent Bonding

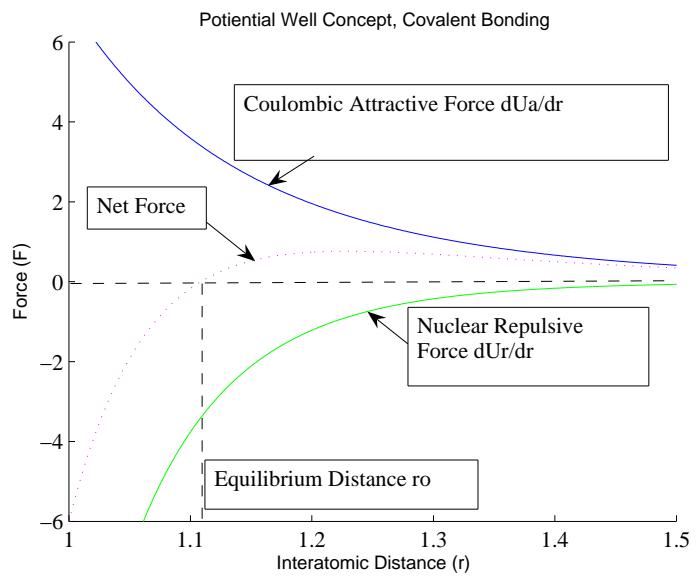


Figure 2: Differentiation of the Potential Energy Well

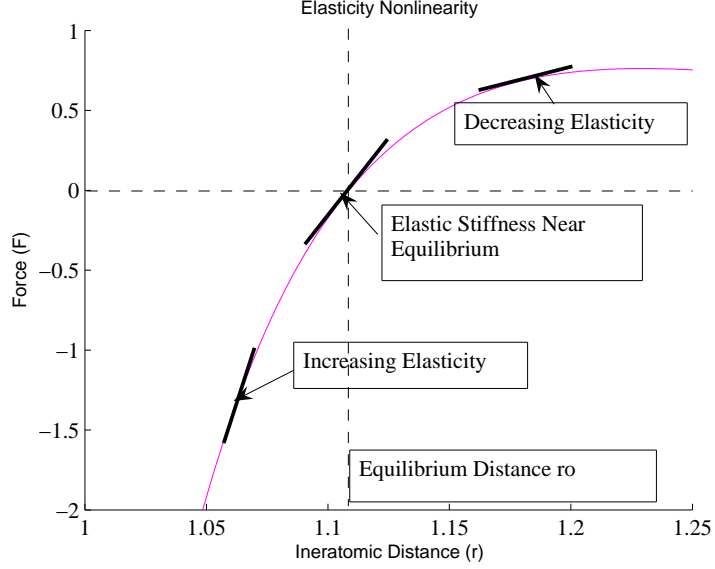


Figure 3: Elasticity Dependence on Strain

Figure 3 shows that as the atoms are brought closer together the slope of the force distance curve increases, corresponding to an increase in “stiffness”. The opposite is seen for an increasing separation distance. Also the relative decrease in elasticity with positive strain is larger than the increase in elasticity with negative strain. The TOEC compensates for the nonlinearity in the bonding stiffness, Eq. 3. Therefore, if the elastic nonlinearity dominates the density effect, the trends in the stiffness nonlinearity should mirror the trends in the acoustoelasticity, with respect to magnitude and sign with strain orientation, and they do.

1.2.2 Derivation of Third Order Elastic Constants

The modern theory of acoustoelasticity was developed by Hughes and Kelly in the 1950’s by including higher order terms in the constitutive stress strain equations [13]. Since then other theories have been developed to account for anisotropy and residual stresses ([5][8][14][20]). The mathematics of these theories is extremely cumbersome and later a simple linear model is used for experimental determination of acoustoelasticity, therefore only the isotropic theory developed by Hughes and Kelly is shown here.

Using a rectangular Cartesian coordinate system with (a_1, a_2, a_3) representing the original point in a body and (x_1, x_2, x_3) representing the final position.

$$x_r = A_r a_r + U_r(a), \quad r = 1, 2, 3 \quad (8)$$

Where Eq. 8 “represents a general infinitesimal strain superimposed upon a homogenous triaxial finite strain with coordinate axis as principle axis” [13] ($U_r(a) \ll A_r - 1$). The Lagrangian strain components are,

$$\begin{aligned} \eta_{rs} &= \alpha_r \delta_{rs} + A_r A_s \epsilon_{rs} \\ \delta_{rs} &= \begin{cases} 1 & \text{if } r = s \\ 0 & \text{if } r \neq s \end{cases} \\ \alpha_r &= \frac{1}{2}(A_r^2 - 1) \\ \epsilon_{rs} &= \frac{1}{2} \left(\frac{\partial U_r}{\partial x_s} + \frac{\partial U_s}{\partial x_r} \right) \end{aligned} \quad (9)$$

where ϵ_{rs} are the infinitesimal strains as determined on a body under a general state of finite strain given by α_r . For an isotropic body, the strain energy is a function of the strain invariants which are defined by,

$$\begin{aligned} I_1 &= \delta_s^r \eta_{rs} \\ I_2 &= \frac{1}{2!} \delta_{su}^{rt} \eta_{rs} \eta_{tu} \\ I_3 &= \frac{1}{3!} \delta_{suw}^{rtv} \eta_{rs} \eta_{tu} \eta_{vw} \end{aligned} \quad (10)$$

Using these strain invariants the strain energy per unit mass can be written as,

$$\phi = \frac{1}{2}(\lambda + 2\mu)I_1^2 - 2\mu I_2 + \frac{1}{3}(l + 2m)I_1^3 - 2mI_1 I_2 + nI_3 \quad (11)$$

where λ and μ are the Lamé constants and l , m , and n are called the Murnaghan constants.

The density is given by,

$$\rho = \frac{\rho_o}{1 + 2I_1 + 4I_2 + 8I_3} \quad (12)$$

where ρ_o is the unstrained density. The stresses, σ , are now written as,

$$\sigma_{rs} = \sigma_{rs}^o + \sum_{tu} C_{rstu} \frac{\partial U_t}{\partial x_u} \quad (13)$$

$$\begin{aligned}\sigma_{rs}^o &= [\lambda + 2(l - m - \lambda)\theta + (\lambda + m - \mu)\alpha_r]\theta\delta_{rs} + \\ &+ 2\mu(\alpha_r + 2\alpha_r^2)\delta_{rs} + m \sum_t \alpha_t^2 \delta_{rs} + \frac{1}{2}n \sum_{tu} \delta_{stu}^{rtu} \alpha_t \alpha_u\end{aligned}\quad (14)$$

$$\begin{aligned}C_{rstu} &= [\lambda + 2(l - \lambda - m)\theta + 2(\lambda + m)(\alpha_r + \alpha_t) - 2\mu\alpha_r]\delta_{rs}\delta_{tu} + \\ &+ [\mu + (\lambda + m - \mu)\theta + 2\mu(\alpha_r + \alpha_s + \alpha_u)] \times \\ &\times [\delta_{rt}\delta_{su} + \delta_{ru}\delta_{st}] + \frac{1}{2}n \sum_v (\delta_{svt}^{rvu} + \delta_{svu}^{rvt})\alpha_v\end{aligned}\quad (15)$$

$$\theta = \alpha_1 + \alpha_2 + \alpha_3 \quad (16)$$

If we assume that we have plane waves traveling in the unit N_s direction,

$$U_r = F_r \left(\sum_s N_s x_s - ct \right) \quad (17)$$

The velocity, c , is given by,

$$Det \left| \sum_{ru} C_{rstu} N_r N_u - c^2 \delta_{st} \right| \quad (18)$$

Finally, assuming uniaxial stress in the x or y direction, wave propagation along the x direction, and T representing a compressive external loading, the velocities for a longitudinal wave propagating parallel to the stress, a shear wave propagating parallel to the stress with particle polarization normal the stress, a longitudinal wave propagating normal to the stress, a shear wave propagating normal to the stress with particle polarization parallel stress, and a shear wave propagating normal to the stress with particle polarization normal stress are Eq. 19, respectively.

$$\rho_o c_{1x}^2 = \lambda + 2\mu - \frac{T}{3K_o} \left[2l + \lambda + \frac{\lambda + \mu}{\mu} (4m + 4\lambda + 10\mu) \right]$$

$$\rho_o c_{2x}^2 = \mu - \frac{T}{3K_o} \left[m + \frac{\lambda n}{4\mu} + 4\lambda + 4\mu \right]$$

$$\rho_o c_{1y}^2 = \lambda + 2\mu - \frac{T}{3K_o} \left[2l - \frac{2\lambda}{\mu} (m + \lambda + 2\mu) \right]$$

$$\begin{aligned}\rho_o c_{2y}^2 &= \mu - \frac{T}{3K_o} \left[m + \frac{\lambda n}{4\mu} + \lambda + 2\mu \right] \\ \rho_o c_{2z}^2 &= \mu - \frac{T}{3K_o} \left[m - \frac{\lambda + \mu}{2\mu} n - 2\lambda \right]\end{aligned}\tag{19}$$

Experimentally measuring any three of these velocities as a function of stress will determine l , m , and n . After the laborious derivation one can see the common longitudinal and shear velocities for an elastic half space by substituting $T = 0$ into Eq. 19, for a given stress orientation. Expressing the acoustoelasticity of a material is rarely done in terms of the Murnaghan constants or any other TOEC terms. The majority of experimental literature uses a simple linear relationship between wave velocity and stress, Eq. 20,

$$\frac{\Delta c}{c_o} = K \Delta \sigma\tag{20}$$

where the orientation of the stress and the type and orientation of the acoustic wave is specified. This simpler form will be adopted for most of the paper for ease of use and comparison with other reported values. The values for the third order elastic constants are calculated and can be found in Section 4.4.

1.2.3 Other Sources of Nonlinearity

Acoustoelasticity is not the only cause for variations in acoustic velocity. As discussed earlier, processing anisotropy and residual stress can cause variations in acoustic velocity comparable to those caused by material nonlinearity. These additional sources of nonlinearity complicate experimentation and physical interpretation.

The presence of residual stress will cause variation in acoustic velocity. The physics of this effect follows the same principles outlined in the material nonlinearity Section 1.2.1. The lattices, under residual stress, will have different elastic properties than the unstressed lattices, this will in turn effect the speed at which a stress wave is propagated.

Another source of nonlinearity is material anisotropy. Material anisotropy is a variation of material properties with direction. Figure 4 [22] show how the crystal orientation effects Young's modulus for aluminum.

Changes in microstructure with service life also cause changes in acoustic velocity. One such cause for velocity variation is the introduction of dislocations in a material. Specifically,

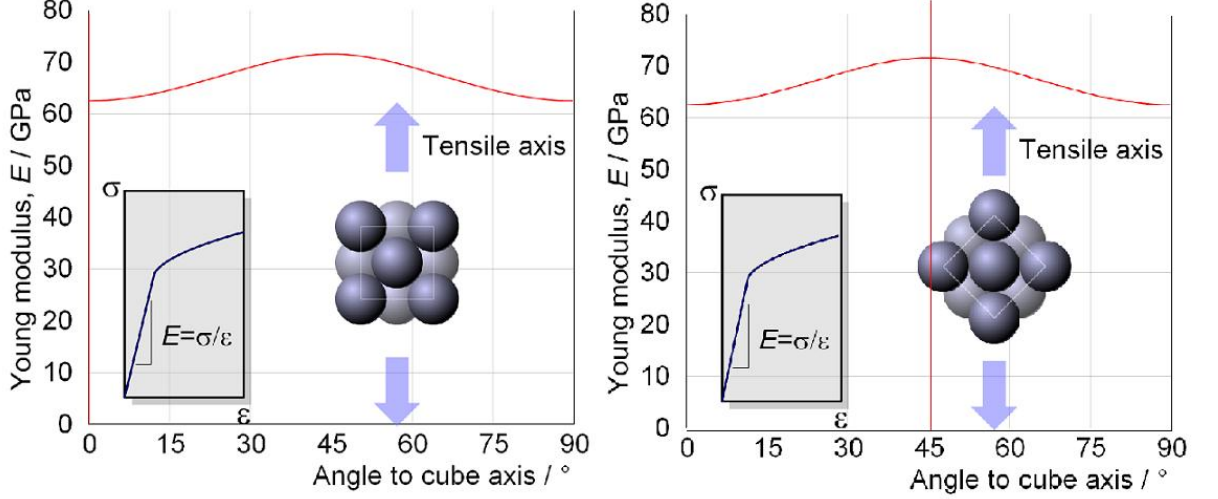


Figure 4: Stress Strain Relationship For A Crystal Orientated Relative To A Uniaxial Loading

a string model for dislocation damping, proposed by Granato and Lucke has been adopted to represent the relationship between velocity change, dislocation density, and dislocation loop length for a line dislocation [11],

$$\frac{c - c_o}{c_o} = -\frac{4Gb^2}{\pi^4 C} \Lambda L^2 \quad (21)$$

where G , b , Λ , L , and C are the shear modulus, magnitude of Burger's vector, dislocation density, dislocation loop length, and dislocation line tension defined by $\frac{2Gb^2}{\pi(1-\nu)}$, respectively. Although this model only addresses one type of dislocation, it is presented to show that models have been proposed correlating velocity changes to material degradation.

1.2.4 2-D Reflection and Refraction Model

Ultrasonic immersion testing is one of the main experimental techniques used in this paper. During immersion testing, the specimen is placed in a fluid filled tank, where the fluid is a medium to couple ultrasonic water between the ultrasonic transducers and the specimen. This technique is advantages because the sample boundary can move without interfering with ultrasonic coupling.

Modeling the reflections and refractions of incident acoustic waves across boundaries will provide a relative energy ratio check for recorded reflections as well as physical insight

into complications that can arise from non normal incident waves.

To begin, we will consider the case of a normal incident longitudinal plane wave at a water aluminum interface. The amplitude of the reflected and transmitted waves, F_r and F_t , respectively, can be written in terms of the amplitude of incident wave, F_i , and a coefficient, Eq. 22.

$$F_r = R \times F_i$$

$$F_t = T \times F_i \quad (22)$$

In Eq. 22, R and T are the reflection and transmission coefficients, respectively, equaling Eq. 23,

$$R = \frac{Z^{AL}/Z^{Water} - 1}{Z^{AL}/Z^{Water} + 1}$$

$$T = \frac{2 Z^{AL}/Z^{Water}}{Z^{AL}/Z^{Water} + 1} \quad (23)$$

where Z^x is the acoustic impedance equaling Eq. 24.

$$Z^x = \rho^x c^x \quad (24)$$

The most complicated geometry used in this paper contains three interfaces of water and aluminum, Fig. 5.

This geometry is used to obtain the time of flight (TOF) through the sample and the thickness of the sample. The first reflection from the front wall is recorded as well as the wave that transmits from water to aluminum at the front wall, reflects from water to aluminum at the back wall, and finally is transmitted from aluminum to water at the front wall. The difference of the TOFs of these two waves will give the TOF for a wave traveling twice through the aluminum. An example of these two pulses is seen in Fig. 6.

The amplitude reduction in the two pulses can be verified using a series of reflection and transmission coefficients. Assuming the amplitude of the incident wave, F_i , is unity, the amplitude of the first reflected wave, F_1 , is Eq. 25,

$$F_1 = 1 \cdot R_{Water}^{AL}$$

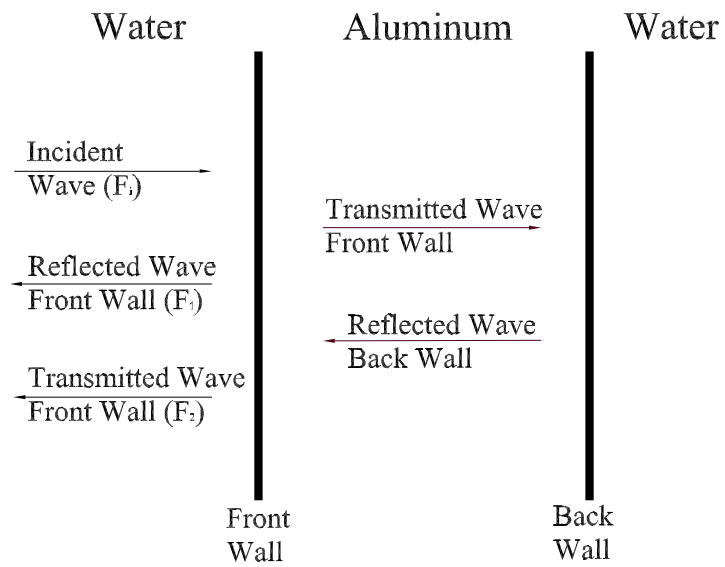


Figure 5: 2D Normal Incident Plane Wave at Multiple Interfaces

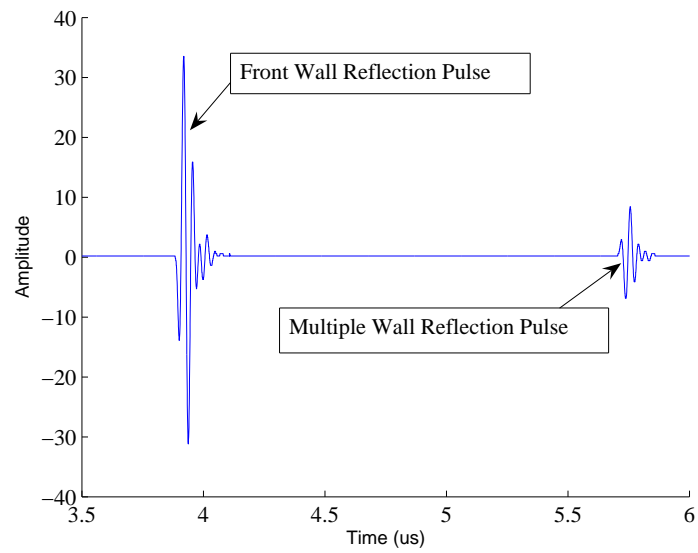


Figure 6: 2D Normal Incident Plane Wave at Multiple Interfaces

$$R_{Water}^{AL} = \frac{Z^{AL}/Z^{Water} - 1}{Z^{AL}/Z^{Water} + 1} \quad (25)$$

where the subscript on R or T denotes the LHS media and the superscript denotes the RHS media in concordance with Fig. 5. The amplitude of the wave which transmits from water to aluminum at the front wall, reflects from water to aluminum at the back wall, and transmits from aluminum to water at the front wall, F_2 , is Eq. 26.

$$F_2 = 1 \cdot T_{Water}^{AL} \cdot R_{AL}^{Water} \cdot T_{AL}^{Water}$$

$$T_{Water}^{AL} = \frac{2 Z^{AL}/Z^{Water}}{Z^{AL}/Z^{Water} + 1}$$

$$R_{AL}^{Water} = \frac{Z^{Water}/Z^{AL} - 1}{Z^{Water}/Z^{AL} + 1}$$

$$T_{AL}^{Water} = \frac{2 Z^{Water}/Z^{AL}}{Z^{Water}/Z^{AL} + 1} \quad (26)$$

Taking the ratio of F_1/F_2 and substituting the proper values for the densities and wave speeds of water and pure aluminum, (Tables 1 and 2), $F_1/F_2 = -3.4$. The negative sign indicates that there is a phase shift. Examining Fig. 6 the peak amplitudes of the pulses are compared and found to have a ratio of ≈ 3.9 . The phase shift is clearly seen in Fig. 6 as the first wavelet of the first pulse is negative and the first wavelet of the second pulse is positive.

Table 1: Acoustic Wave Velocities of Aluminum and Water [9].

Aluminum		Water at 20 C°	
Longitudinal	Shear	Longitudinal	Shear
6320 m/s	3130 m/s	1480 m/s	null
0.249 in/ μ s	0.123 in/ μ s	0.058 in/ μ s	null

There is more amplitude reduction in the experimental data than was predicted by theory. However, this is to be expected for several reasons.

One cause is attention, where some energy is absorbed by intermolecular thermal viscosity effects and some energy is scatter by grains and other microscopic irregularities. There is also a wave spreading affect which causes energy reduction with distance.

Table 2: Densities of Aluminum and Water [1].

Density	
Aluminum	Water at 20 C°
$2.700 \times 10^3 \text{ kg/m}^3$	$0.998 \times 10^3 \text{ kg/m}^3$
$97.544 \times 10^{-3} \text{ lb/in}^3$	$36.055 \times 10^{-3} \text{ lb/in}^3$

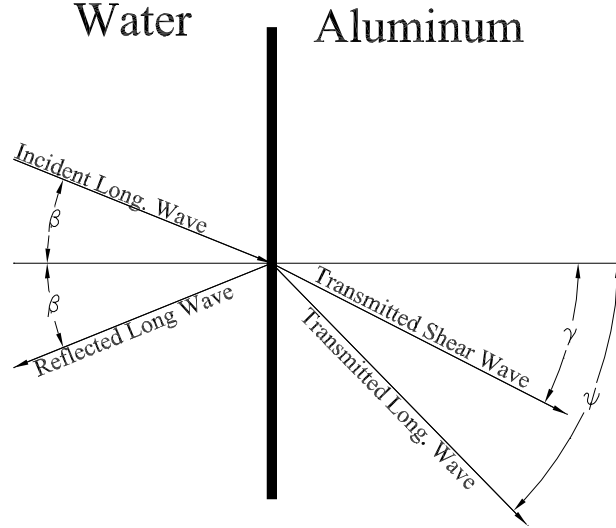


Figure 7: 2D Non Normal Incident Plane Wave at an Interface

Another cause is that in experimental testing the incident wave is not truly normal to the interface. This issue caused a great deal of experimental difficulty, as will be explained later, and can rarely be fully corrected.

If the incident wave is off normal by an angle β , the 2-D single boundary layer problem becomes more complicated and the multilayered boundary problem becomes much more involved. To illustrate this, the 2-D single boundary problem is diagramed in Fig. 7.

The angled incident wave produces both a longitudinal wave and a shear wave in the aluminum layer. There is only longitudinal waves in the water because fluids are unable to support shear wave motion.

The reflection and refraction angles can be determined using Snell's law or the trace velocity matching theory, Eq. 27.

$$\frac{\sin \theta_1}{c_1} = \frac{\sin \theta_2}{c_2} \quad (27)$$

The fluid reflected wave is at the same angle as the incident wave, as c_1 and c_2 are equal. The transmitted waves, however, will be at an angle proportional to c_{AL}/c_{water} . This velocity mismatch causes the angle to increase through the sample by about 4 times for longitudinal and 2 times for shear. This velocity mismatch is a further detriment in calculating the TOF and thickness because any non normal incident angle is magnified at the interface. This issue will be addressed more thoroughly in the experimental chapter.

In terms of the experimental geometry depicted in Fig. 5, the off normal incident wave is rather involved to fully model. A number of mode conversions and polarizations can occur in the solid depending on the incident angle and the subsequent angles of reflection and refraction. In terms of experimentation, the incident wave angle will be controlled and minimized so that the normal incident model can be used, within uncertainty.

CHAPTER II

EXPERIMENTATION

2.1 *Aluminum Specimens, Fatiguing, and Ultrasonic Equipment*

The goal of the following experimentation is to determine the acoustoelastic constants and TOEC of 7075-T651 aluminum and to correlate these parameters with fatigue damage. The following sections will detail the specifics of the samples used, how the samples were damaged, and what kinds of ultrasonic equipment was used.

2.1.1 Sample Description

All experiments were performed on rectangular dog-bone specimens of the dimensions detailed in Fig. 8.

The mechanical properties for general 7075-T6 aluminum are found in Table 3 [9].

Table 3: Mechanical Properties for 7075-T6 Aluminum

7075-T6 Aluminum				
Elastic Modulus	0.2% Yield Strength	Ultimate Strength	Poisson's Ratio	Crystal Structure
E GPa (10^3 ksi)	σ_o MPa (ksi)	σ_y MPa (ksi)	ν	
71 (10.3)	469 (68)	578 (84)	0.345	FCC

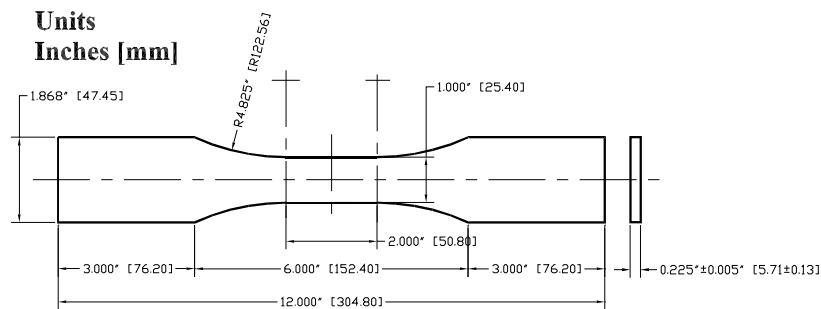


Figure 8: Engineering Drawing of Dog-bone Samples

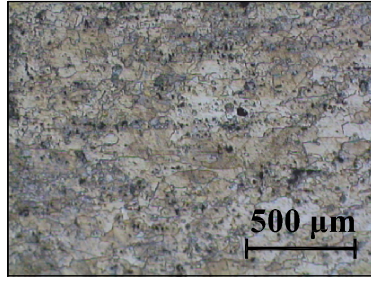


Figure 9: Microstructure of a Plane Perpendicular to Rolling Direction

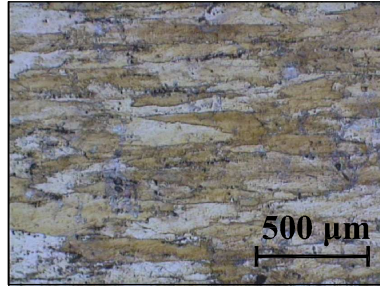


Figure 10: Microstructure of a Plane Parallel to Rolling Direction

The samples were processed by cold rolling along the axis that the uniaxial loading will be applied.

Sections, in the gauge area, of a fatigued and unfatigued sample were analyzed metallographically. Sections were taken parallel and perpendicular to the rolling direction and can be seen for an undamaged sample in Figs 9 and 10.

The sectioned specimens were mounted using Bakelite, ground using SiC paper progressing incrementally from 120 to 800 grit, polished using alumina (Al_2O_3) powder, $2\mu m$, $0.5\mu m$, and $0.05\mu m$ concentrations sequentially, and finally etched using Keller's etching reagent.

In terms of microstructure, it is clear that there is grain elongation in the direction of the rolling. The grain structure perpendicular to the rolling direction appears to be uniform along the thickness of the sample.

Similar cross section were taken from a sample fractured under fatigue damage. The sections were taken near the fractured area and no appreciable change in microstructure was seen.

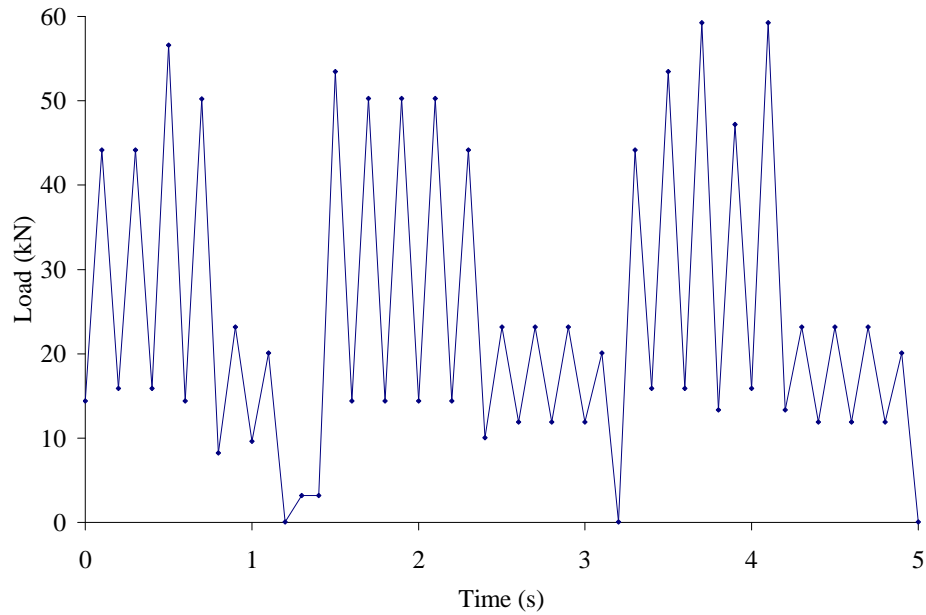


Figure 11: Portion of Fatigue Loading Spectrum

2.1.2 Fatiguing

Samples were fatigued to different degrees of life in order to correlate ultrasonically measured parameters with fatigue life. The samples were fatigued using a uniaxial fatigue machine operating with MTS testing software.

The load schedule consists of 2640 unique tension-tension cycles. This load schedule, called a block, is then repeated as necessary. The first 5 seconds of the loading spectrum can be seen in Fig. 11.

The loading frequency is 5 Hz with an average peak loading of 56000 N. This corresponds to a peak stress of 385 MPa, about 80% of the yield stress. Thus the general failure mechanisms is expected to be yielding dominated [9].

One sample was run until failure and its fatigue life was found to be 52,800 cycles or 20 blocks. The results were also supported by a Palmgren-Miner model.

This fatigue life is used as a base when samples are referenced to the percent of fatigue life they have been damaged. However, due to processing and material inhomogeneities, samples can vary in fatigue life by 1000's of cycles. Therefore if a sample is said to be

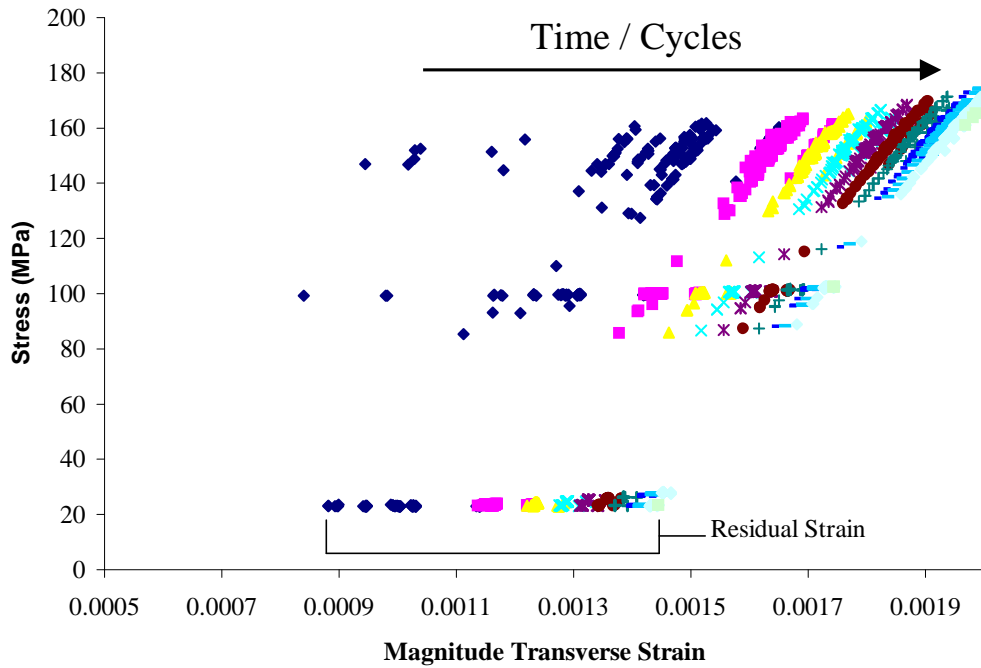


Figure 12: Computed Stress vs Strain during Fatiguing using MTS output

fatigued 80 percent of its life, this should be taken as an estimation.

During the fatiguing of a sample, to 40 percent life, force, displacement, and time data was recorded using the MTS software. The force and displacement data was used to generate a stress strain plot and is shown in Fig. 12.

It should be noted that the strain data is not precisely accurate as the displacement is taken over the whole of the sample, and thus the stress and strain recorded is the integrated effect over the whole geometry of the sample, not the gauge section alone, which is where ultrasonic analysis is performed. However the general trend should be representative of the of the gauge section stress and strain.

In Fig. 12, the different symbols represent the fatigue blocks. There is an increase in plastic strain throughout the fatiguing processes, as seen by the residual in the strain axis. As the fatigue process progresses, plastic strain hardening causes the growth rate of this residual to decrease.

2.1.3 Ultrasonic Testing Equipment

2.1.3.1 Ultrasonic Transducers

Two main types of ultrasonic transducers were used while determining the acoustoelastic constants. All transducers used, however, generate mechanical waves using piezoelectric elements and were manufactured by Panametrics.

Measurement of the longitudinal acoustoelastic constants and strain mapping was performed using 20 MHz unfocused immersion transducers. Specifically, a pair of Panametrics video scan model V316 transducers with 0.125 inch elements were used, serial numbers 504389 and 504388.

The longitudinal transducers, described above, are designed to use a fluid as a coupling agent and measurements were made in an immersion tank.

Measurement of the shear acoustoelastic constants was performed using a 5 MHz contact transducer. Specifically, a video scan shear transducer by Panametrics, model V220-BA, with a 0.25 inch element size is used, serial number 51557.

The shear wave transducer was coupled to the specimen using a honey glycerine couplant made by Panametrics. The couplant was able to provide transmission of a normal incident shear wave to the specimen.

2.1.3.2 Ultrasonic Hardware

The general setup for generating and recording ultrasonic waves in the specimens is diagrammed in Fig. 13.

The pulser receiver used was a “200 MHz Computer Controlled Pulser Receiver” model 5900 PR made by Panametrics. The pulser receiver is controlled with “Scan View Plus” a software package designed by Panametrics. The software package acts as a digital oscilloscope, showing the current wave form in “digitized real time”.

2.1.3.3 Ultrasonic Scanning System

The longitudinal acoustoelastic constants and strain mapping experimentation were performed with an immersion scanning ultrasonic system. The scanning system was custom

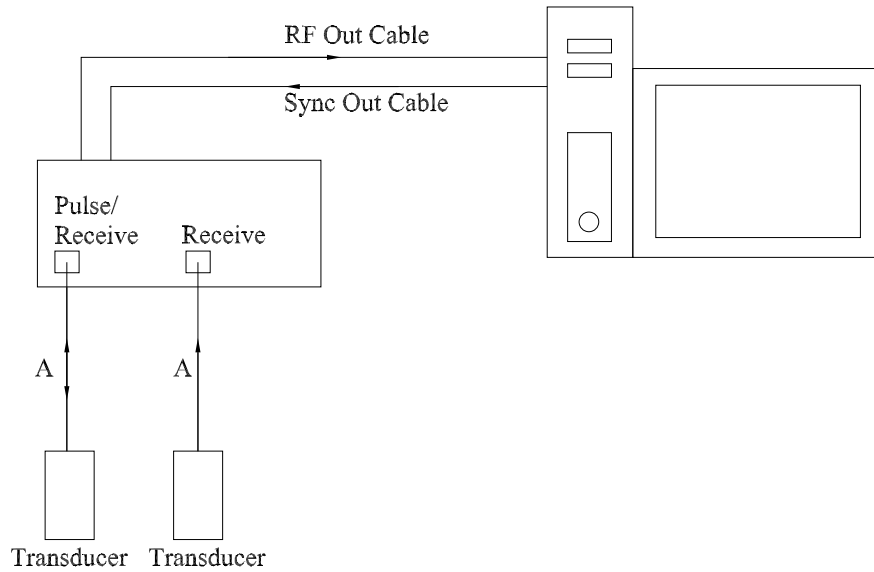


Figure 13: System for Generating and Recording UT Waves

designed by Panametrics, it has 5 motion axes, and is controlled with the Panametrics’ “Scan View Plus” software.

The scanning arm is capable of motion in three direction, x, y, z . The head piece of the arm is capable of rotating about it’s z axis (swivel) and rotating about a line perpendicular to it’s z axis (gimbal).

The scanning head is outfitted with a yoke attachment. The yoke attachment is capable of housing two transducers and is shown in Fig. 14.

2.2 Immersion Testing: Experimental Setup for Longitudinal Acoustoelastic Constants and Strain Mapping

The following will detail the specific experimental setup for determining longitudinal acoustoelastic constants and strain mapping. One of the main focuses of the section will be the nature of the geometrical errors present in the proposed experimental technique and how these errors were corrected.

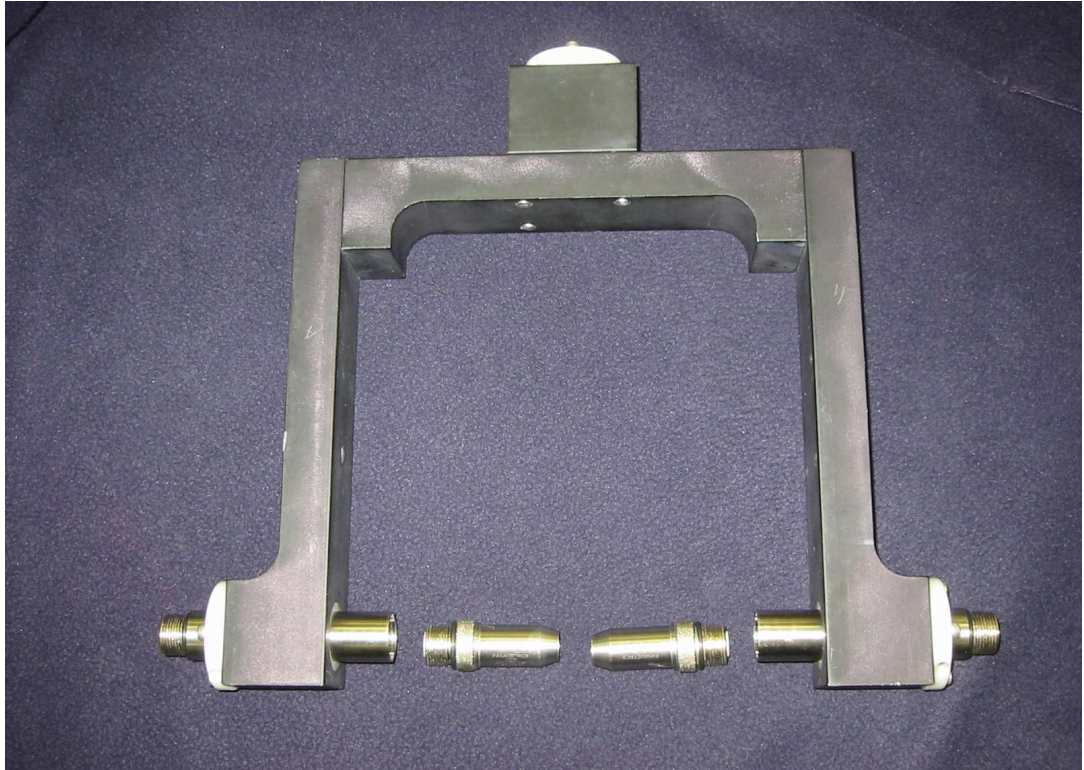


Figure 14: Yoke Attachment and Transducers

2.2.1 Experimental Setup

Measuring the acoustoelastic constants requires a system in which the acoustic velocity can be measured as a function of applied stress. Velocity is defined in Eq. 28.

$$Velocity = \frac{Distance}{Time} \quad (28)$$

Time is the TOF required for an ultrasonic wave to travel through the sample and the distance is the dimension of the sample that this wave has traversed.

This particular experiment is concerned with a longitudinal wave traveling traverse to the applied loading through the, 5.7 mm, thickness of the sample.

A static loading fixture, designed by a colleague, Dr. Bao Mi (Fig. 15), was used in order to place the sample under uniaxial stress.

A hydraulic cylinder is attached at the indicted location and an external pump is used for displacement control. A load cell is placed in between the sample and the pump shaft. This load cell has an output to a digital “Panel Meter”, model DP25-S by Omega.

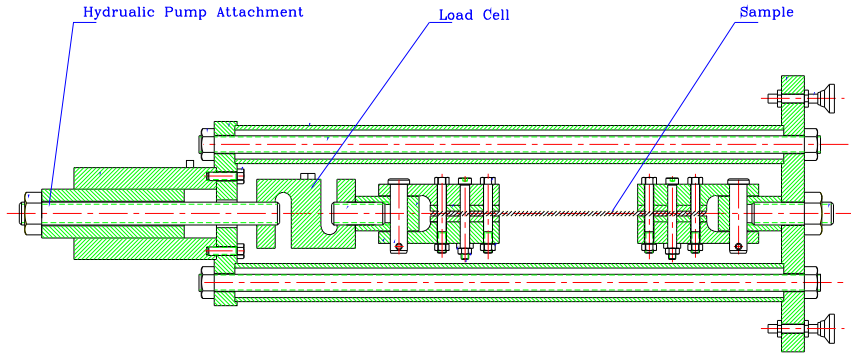


Figure 15: Static Loading Fixture

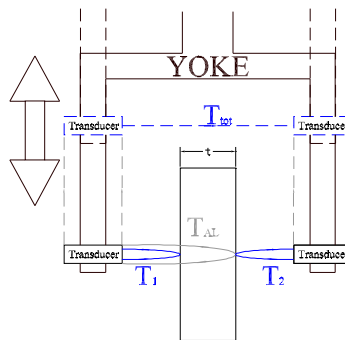


Figure 16: Yoke, Transducer, Specimen Setup

A method is now needed for measuring ultrasonic TOF and sample thickness while the sample is in the loading fixture. These two tasks can be accomplished simultaneously by placing the loading fixture in the immersion tank and using the yoke attachment for the scanning head. Figure 16 shows how measuring four specific reflections can achieve this goal. A picture of this setup in the scanning tank is seen in Fig. 17.

Recording the four wave reflections labeled in Fig. 16 will provide all of the information needed to determine the sample thickness, t , and the TOF of an ultrasonic wave traveling through the thickness.

First, the head is raised in the z axis so that the sample is no longer obstructing the path of the transducers. One transducer is pulsed and the adjacent transducer receives

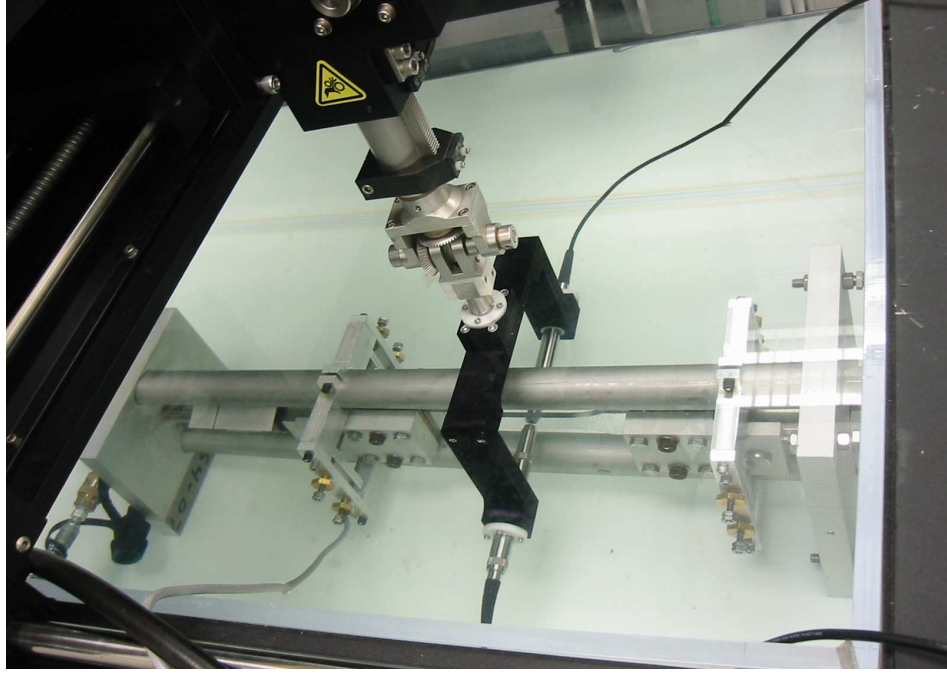


Figure 17: Yoke, Transducer, Loading Fixture, Specimen Setup

the signal. This TOF, labeled T_{tot} in Fig. 16, is used to determine the total unobstructed distance between the transducers in the yoke. Now the head is lowered so that the sample is obstructing the wave path. Pulse echo waveforms are recorded on each transducer, T_1 and T_2 in Fig. 16. The first received pulse will have traverse the distance from the transducer to the face of the sample twice. The total distance between the two transducers and the distance between each transducer and the adjacent sample face can be determined with Eq. 29.

$$\begin{aligned}
 D_{tot} &= (c_{L,water})T_{tot} \\
 D_1 &= \frac{1}{2}(c_{L,water})T_1 \\
 D_2 &= \frac{1}{2}(c_{L,water})T_2
 \end{aligned} \tag{29}$$

Subtracting the two transducer distances from the total distance will give the sample thickness, $t = D_{tot} - D_1 - D_2$. The sample can then be strained, using the loading fixture, and this process is repeated. This will be the general technique used for the velocity measurements. The setup geometry errors and the specific signal processing techniques will be

explored later.

The TOF, through the thickness of the sample, can be calculated by including one other reflection in the pulse echo measurement. Figure 16 shows an extended wave path for one of the transducers. The path labeled T_{AL} represents an ultrasonic wave that is transmitted through the front wall of the sample, reflected off the back wall of the sample, and transmitted through the front wall again (Note: This model was outlined in detailed in Fig. 5). In terms of Fig. 16, $T_{AL} - T_1$ will leave the TOF for an ultrasonic wave which has made two passes through the sample thickness. We now have the TOF through the sample.

This setup allows for measurement of the acoustic phase velocity (longitudinal in this case) as a function of applied load.

2.2.2 Tooling and Techniques Aimed at Reducing Geometric Errors

One of the greatest difficulties, in measuring load dependent velocities, is the high level of accuracy that is needed. The acoustoelastic effect is very small, typically of the order 0.001% per MPa of applied stress, for metals.

2.2.2.1 Aligning Ultrasonic Wave Path Normal to Sample

The digitizing frequency used is 2 GHz, corresponding to a time resolution of 0.5 ns. This resolution can be improved using signal processing techniques, discussed later, and is adequate for acoustoelastic measurements.

The main source of error arises from non normal sample transducer geometry. If the propagating wave direction is not normal to the sample face, the path length measured will increase thus leading to inaccurate distance measurements, Fig. 18.

The non normal interface in Fig. 18 must be extended to 3 dimensions, such that the gimbal axis may be off normal as well.

Both of these effects can be corrected for by performing a scan along the sample using the swivel and gimbal motion of the scanning head. When the transducers wave path is normal to the sample the reflection scatter will be minimized and the signal energy will peak.

Positioning the transducer face normal to the sample can be done by scanning the swivel

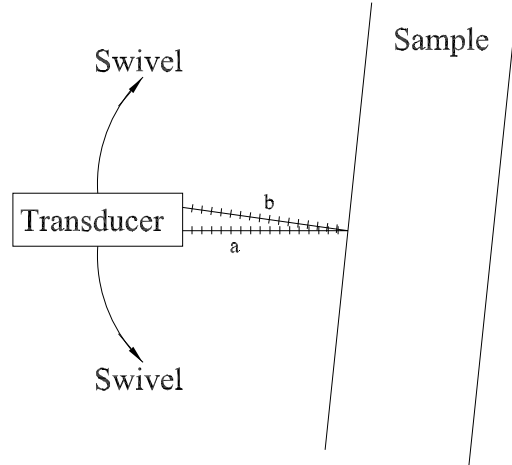


Figure 18: Model of Angle Error

and gimbal. To begin the swivel and gimbal are manipulated to visually peak the pulse echo signal amplitude. Next, this angle is assigned the value of zero. A B-scanning sequence is then executed from -2° to $+2^\circ$, in the swivel and gimbal, recording waveforms every 0.01° . The energies are then plotted versus swivel and gimbal angle and a second order polynomial is fit to the data. The peak of the parabolic function is found with one differentiation and the corresponding angle is recorded, Fig. 19.

2.2.2.2 Maintaining Normal Wave Paths During Static Loading

Using all of the geometric corrections outlined below, the thickness and TOF can be confidently measured while statically loading the sample.

After the transducers have been aligned normal to the sample face they must be kept normal during loading. The orientation of the sample in the static loading fixture is a function of applied load. This effect is caused by a non collinear loading axis with respect to the centroid of the sample, Fig. 20. Thus under loading the specimen may move, due to play in the mounting design of the loading fixture.

Specific tooling was designed in order to stabilize the motion of the sample under loading and to level the sample prior to loading. A leveling fixture was designed to clamp onto the loading fixture and then control the orientation of the sample with eight steel contact points,

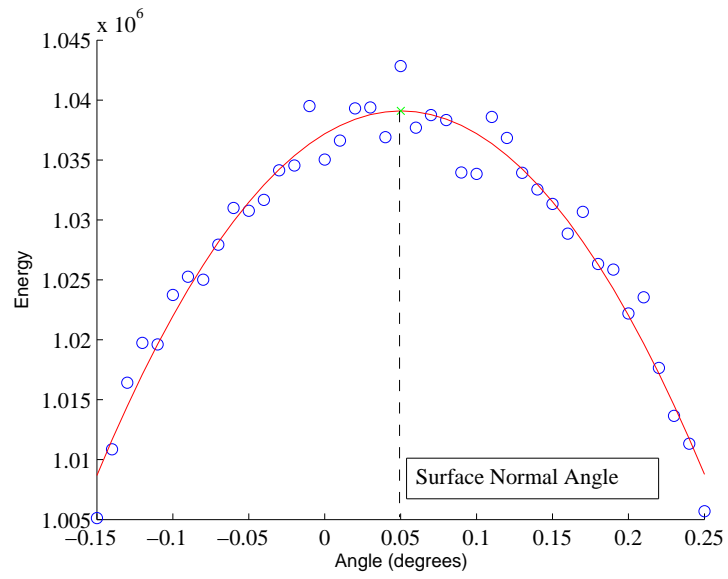


Figure 19: B Scan for Finding Normal Angle

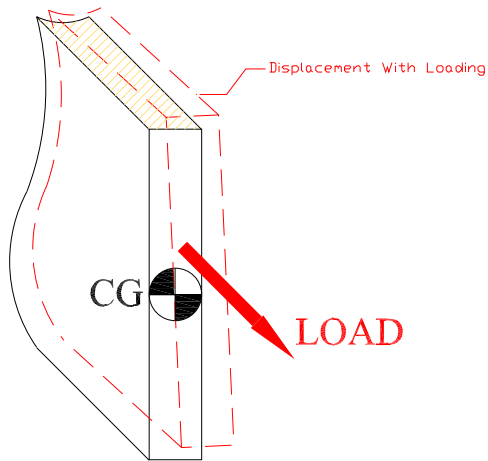


Figure 20: Sample Distortion under Off CG Loading

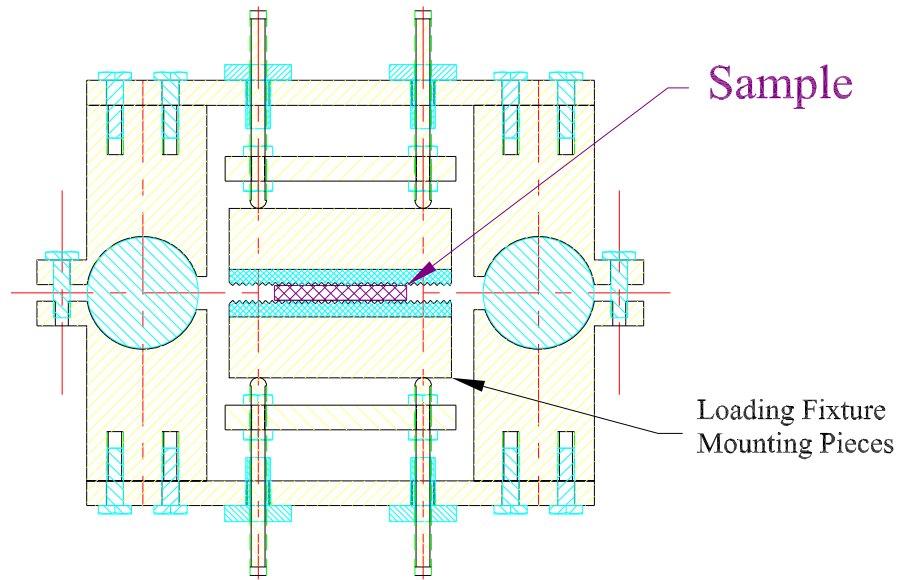


Figure 21: Leveling Fixture: Section

which can be adjusted linearly, Figs 21,22 and 17.

Differential threaded adjusting screws were used to increase the linear precision of each contact rod. The contact rods were made of stainless steel $\frac{1}{4}$ – 28 threaded rods. These rods were threaded through housings which have an external $\frac{3}{8}$ – 24 threading and an internal threading of $\frac{1}{4}$ – 28. The external housing then screws into the holding plate on the leveling fixture, Fig. 23.

Turning a 24 threads per inch screw one revolution causes 0.042 *inches* (1.067 *mm*) of linear motion ($\frac{1}{24} \approx 0.042$), turning a 28 threads per inch screw one revolution causes 0.036 *inches* (0.9144 *mm*) of linear motion ($\frac{1}{28} \approx 0.036$). With the differential, one turn of the external housing results in $0.042 - 0.036 \approx 0.006$ *inches* (.153 *mm*) of linear motion for the contact rod. Attaching the leveling fixture to the loading fixture allows precise positioning of the sample relative to the loading fixture.

The final leveling task is to orient the sample squarely in the loading fixture so that its surface is flat, parallel and perpendicular to the loading direction. This was accomplished

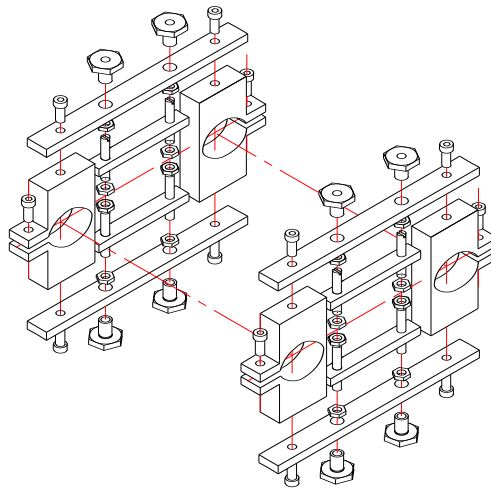


Figure 22: Leveling Fixture: Assembly

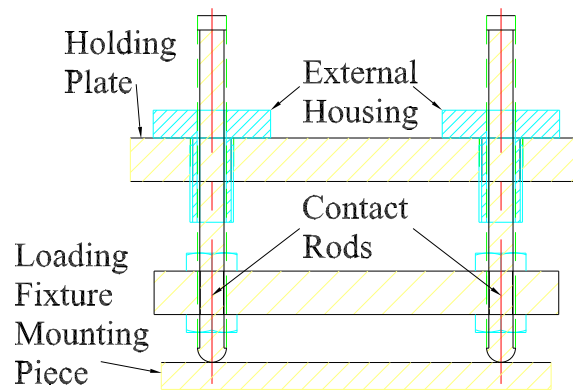


Figure 23: Leveling Fixture: Thread Differential and Contact Rods

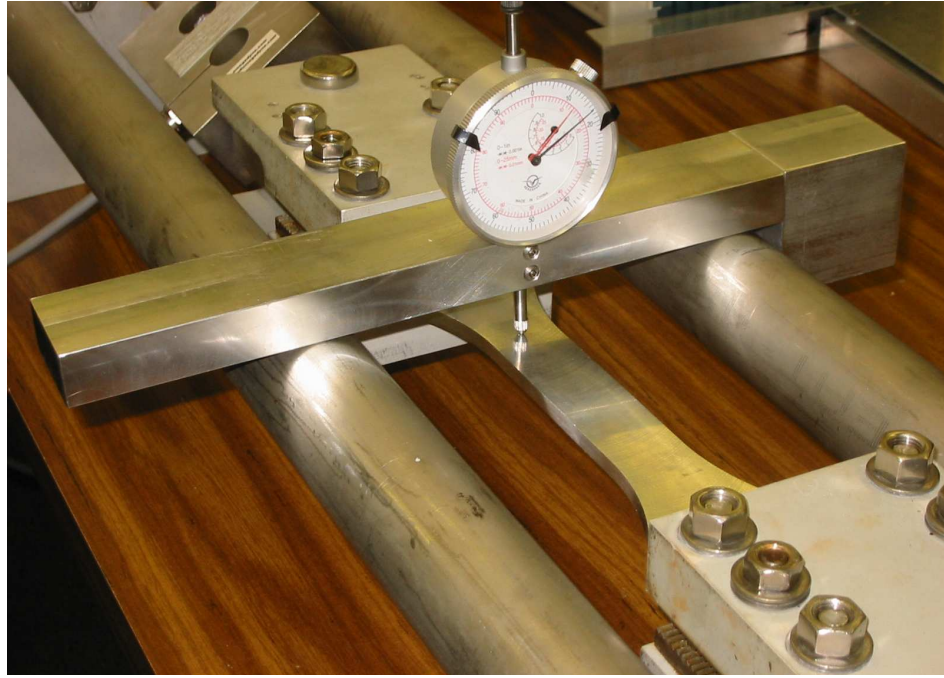


Figure 24: Sample Leveling with Dial Indicator

by running a dial indicator along the face of the surface to be leveled. The indicator was mounted on a specially designed guide bar, Fig. 24.

The guide bar rest on the two main structural rods of the loading fixture, Fig. 15, and is manually moved along the sample.

After implementation of the leveling fixture the total angular dependence on load is reduced to no more than 0.2° for every 4500 N of applied force (the typically experimental load increment).

In order to assure accuracy, the distance of the transducer to the sample must be small enough that this angular error is less than the associated strain. At 4500 N the traverse strain is $\epsilon = \frac{\delta t}{t_0} \approx 0.00016$, therefore the δt that is trying to be measured is $5.715 \text{ mm} \times 0.00016 \approx 1.0 \text{ } \mu\text{m}$. Therefore the maximum allowable error is $0.1 \text{ } \mu\text{m}$, at 10 percent accuracy. The angle error is analyzed with a simple geometric model, Fig. 25.

This error, in terms of Fig. 25, can be used to determine how close the transducer must be to the sample, b .

$$\text{error} = a - b$$

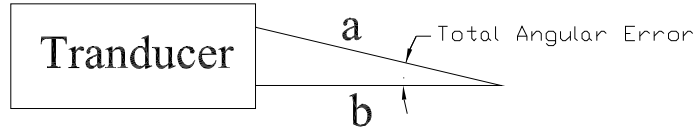


Figure 25: Simply Model of Angle Error

$$\begin{aligned}
 b &= a \times \cos(\theta) \\
 error &= b \times \left[\frac{1}{\cos(\theta)} - 1 \right] \\
 b &= (error) \times \left\{ - \frac{\cos(\theta)}{[\cos(\theta) - 1]} \right\} \tag{30}
 \end{aligned}$$

Using the 10 percent error of $0.1 \mu m$ and a total angle error, θ , of 0.2° , b , the distance of the transducer to the sample, is found to be $\approx 16.5 \text{ mm}$ or $\frac{1}{10} \text{ inch}$.

Using all of the geometric corrections outlined above, the thickness and TOF can be confidently measured while statically loading the sample.

2.3 Longitudinal Acoustoelastic Constants and Strain Mapping

Four dog-bone specimens were used for determination of the longitudinal acoustoelastic constants and building of a stress strain relationship.

2.3.1 Longitudinal Acoustoelastic Constants

The experimental setup used for obtaining TOF and thickness measurements, using an immersion tank, is outlined in Section 2.2.1. The following will cover the specifics of the experimental runs.

To begin, each sample was base lined to determine the acoustoelastic constant in an undamaged state and to explore variations due to experimental error and sample inhomogeneities.

Each sample is properly mounted and leveled. The sample and loading fixture are then placed in the immersion tank. The longitudinal immersion transducers are placed in the yoke. Several B-scans are then performed in order to align the transducers normal to the

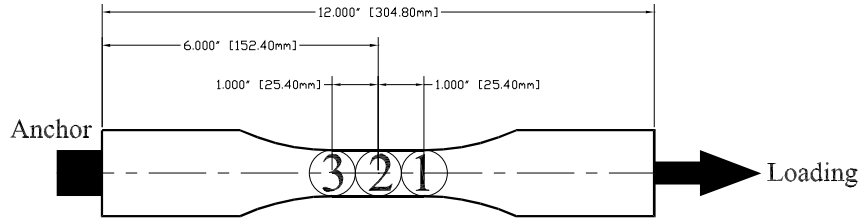


Figure 26: Location of Measurements

sample. The transducers are then moved to the appropriate spacing, with respect to the sample, and locked into position using two nylon tipped set screws.

The following parameters and their typical values are set on the 5900 pulser receiver, Table 4.

Table 4: Typical Pulser Receiver Settings

5900 Pulser Receiver Settings				
Pulse Repetition Frequency	Energy	Damping	High Pass Filter	Low Pass Filter
5 kHz	2 μJ	50 ohm	1 MHz	100 MHz

Attenuation and gain is set case by case such that the signal fills the entire screen, maximizing bit resolution. Using “Scan View Plus”, the following acquisition and digitizing parameters are set, Table 5.

Table 5: Typical Scan View Plus Acquisition Settings

Scan View Plus Acquisition Settings			
Digitizing Frequency	Coupling	Waveforms Averaged	Time Gate (typ)
2000 MHz	50 ohm DC	500	0 – 10 μs

The data acquisition sequence is as follows. Move scanning arm to position 1, Fig. 26. Position scanning head so that the path between the transducers is unobstructed and record the through transmission for transducer 1 to transducer 2, Fig. 27. Position the scanning head so that the sample is in between the two transducers and record pulse echo signals from each transducer, Figs. 28 and 29.

Increment load a random amount (near 4000 N), record load, record pulse echo signals

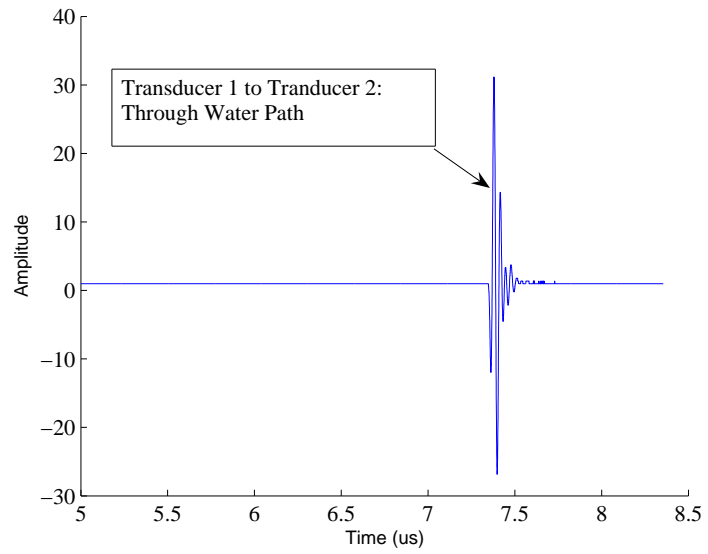


Figure 27: Typical Ultrasonic Signal for Through Transmission From Transducer 1 to Transducer 2

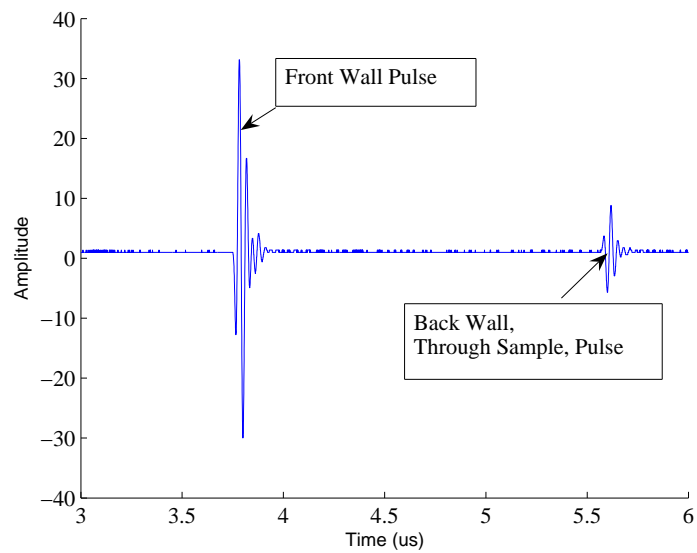


Figure 28: Typical Ultrasonic Signal for Pulse Echo Transducer 1

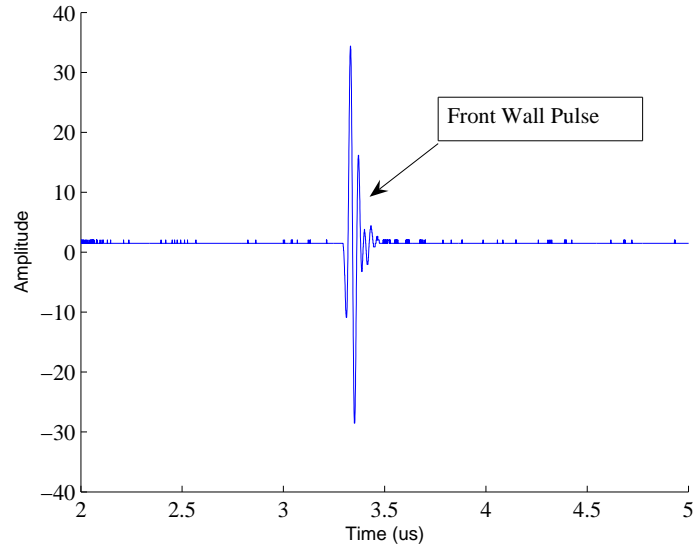


Figure 29: Typical Ultrasonic Signal for Pulse Echo Transducer 2

from each transducer, and repeat until the load has reached 53380 N. Remove the load from the sample.

This process is repeated three times at location 1. The scanning arm is then moved to location 2, and the same sequence is executed. The same is done for position 3.

This sequence is repeated for all four samples. Each sample is then fatigued to the estimated percentage of fatigue life shown in Table 6.

Table 6: Fatigue Damage Of Each Sample

	Sample Identification Number			
	S4-0040	S4-0039	S4-0038	S4-0037
Fatigue Cycles	0	19,680	29,520	39,360
Fatigue Life	0%	40%	60%	80%

After fatiguing, the samples are measured again, in the manner outlined above.

2.3.2 Strain Mapping

The strain may be mapped by measuring the thickness changes in the specimen as a function of applied load.

2.4 Contact Transducer Testing: Shear Acoustoelastic Constants

The shear wave acoustoelastic constants are measured using contact transducers and the stress strain relationship, found in the longitudinal tests. There must be contact between the transducer and the sample, via a couplant capable of supporting shear wave motion, in order to propagate shear waves in a specimen. Fluids are unable to support shear waves, therefore the experimental technique outlined in Section 2.2.1 can not be used. The difficulty in measuring acoustoelastic constants with contact transducers is that only the TOF can be measured by the transducer, while the thickness must be determined by other means. Fortunately, a great deal of effort was spend tracking the thickness dependence on stress in Section(2.3) and these results can be used here.

2.4.1 Contact Testing: Experimental Setup

In general, there are two types of shear waves, vertically and horizontally polarized. The particle motion direction, with respect to the wave propagation direction, defines the polarization. For the purpose of this experimentation the polarization directions will be defined in terms of the uniaxial loading direction. Shear waves will be generated with particle motion parallel with, and perpendicular (normal) to, the direction of loading. The particle motion, for this shear transducer, is defined by the direction of the microdot connector. The transducer is aligned according to Figs. 30 and 31, in order to generate particle motion parallel and perpendicular to the stress.

A pulse echo reading is taken at each load increment. The pulse echo waveform contains reflections from the front wall/couplant interface and from the back wall of the specimen. These two pulses will be used to determine the TOF through the specimen, Fig. 32.

A variety of coupling substances were tried, but ultimately a honey glycine (Panametrics, NPD-053-8002) was chosen for it's repeatability. The transducer is clamped using a rubber tipped C-clamp, Fig. 33, and the ultrasonic signal is monitored until all extra couplant is squeezed out and a uniform bond is left.

The major source of error, when performing contact ultrasonics, is re-bonding. If the

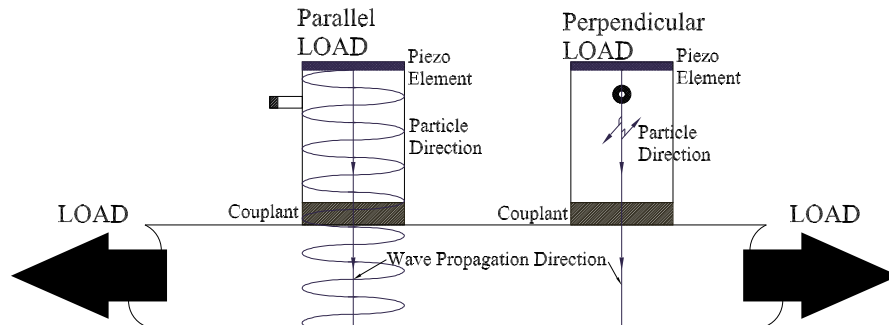


Figure 30: Shear Transducer Orientation to Generate Parallel and Perpendicular Waves

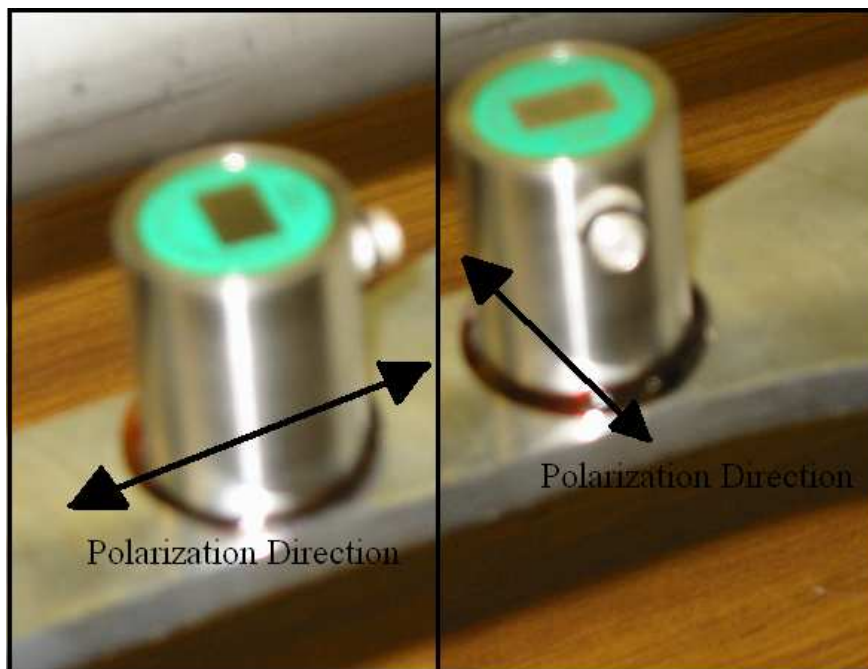


Figure 31: Shear Transducer Polarization

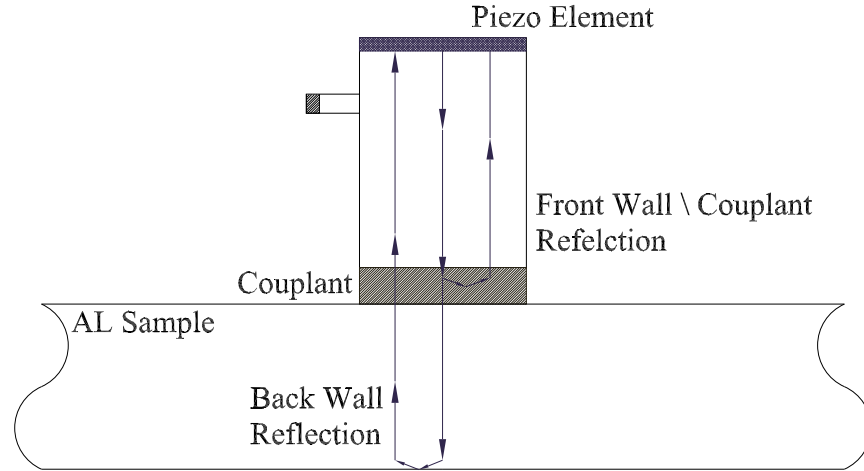


Figure 32: Recorded Reflections for Shear Wave Transducer

location of the transducer, orientation of the transducer, or sample need to be changed, the transducer must be removed and re-bonded (coupled). The specific geometry, consistency, and pressure of the bond can have an enormous influence on the signal content. The exact wave polarization is another error introduced by re-bonding. The alignment of the microdot connector determines the direction of particle motion and cannot be repeated exactly without special tooling.

In order to test the couplant repeatability, the shear transducer was bonded, removed, and re-bonded to a sample, at the same location, three times. For each bond one loading sequence with intermittent TOF measurements was carried out. The results are shown in Fig. 34.

It is clear that there is an offset in the TOF due to the bonding condition. However, the change in TOF with loading is fairly consistent.

2.4.2 Shear Acoustoelastic Constants

The pulser receiver and acquisition parameters are the same as for the longitudinal experiment, with the simplification that only one pulse echo transducer, is needed.



Figure 33: Rubber Tipped Clamp for Mounting Shear Transducer

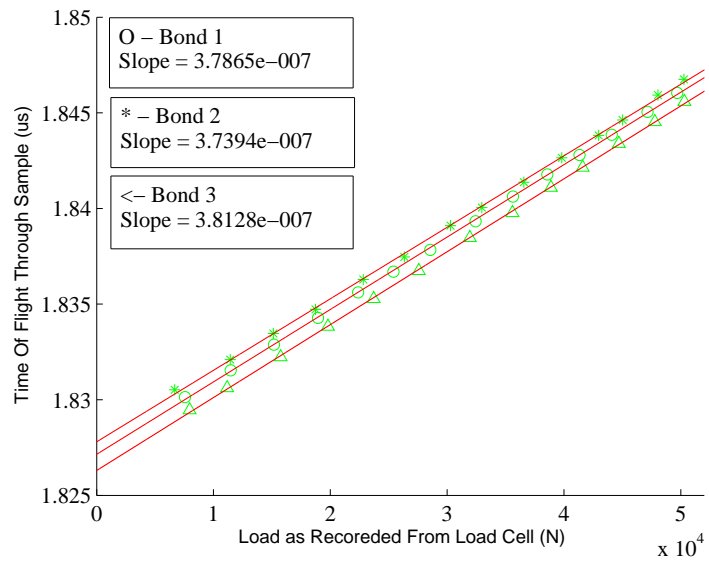


Figure 34: Bonding Consistency Test

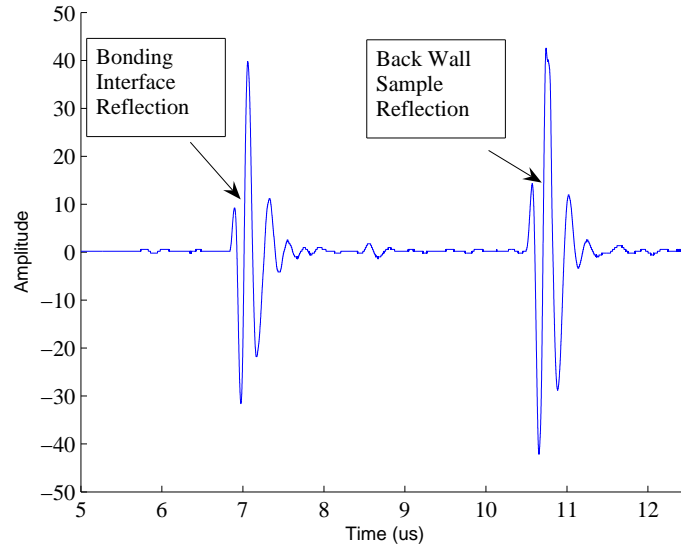


Figure 35: Typical Ultrasonic Signal for Shear Transducer

The shear wave transducer is coupled to the sample using a honey couplant with the orientation of the transducer set to generate waves in the desired polarization direction. Once securely bonded, the signal acquisition is carried out much in the same manner as the immersion test. The transducer is placed at location 1. The load is incremented a random amount (near 4000 N), the load is recorded, a pulse echo waveform is recorded, Fig. 35, and repeat until the load has reached 53380 N. The load is then removed and this sequence is repeated three times.

After the three load series are completed, the C-clamp is removed and the transducer is rotated 90°, to change the direction of polarization, and the C-clamp is reapplied. The signal is monitored until it reaches steady state. Once the signal is at steady state, another three load series is performed using the methodology described above. This procedure is repeated for each of the three locations.

This sequence is repeated for all samples. However, this test was performed after the samples had been fatigued. Therefore, there is a complete data set for an undamaged sample and for several samples at different level of fatigue life.

CHAPTER III

DATA ANALYSIS AND SIGNAL PROCESSING

This chapter will deal with the specific techniques used for analyzing the raw ultrasonic data. The specific signal processing algorithms are described in detail. This chapter will give a thorough overview of all the data obtained and the fundamental parameters derived from this data.

3.1 Immersion Testing: Longitudinal Acoustoelastic Constants and Strain Mapping

Three pulse echo and one through transmission waveforms were measured at various static loads, as outlined in Section 2.2.1, during the immersion testing. Using these waveforms, the thickness of a specimen and the TOF through a specimen, as a function of stress, can be measured. Using these measured parameters, the velocity, as a function of stress, and a stress strain relationship can be derived.

The ultrasonic waveforms are digitized and recorded using the Panametrics' "Scan View Plus" software and saved as .txt files. These text files are then converted into .MAT files, using a code developed by a colleague, Adam Cobb, for signal processing in MatLab.

3.1.1 Longitudinal Acoustoelastic Constants: TOF and Thickness

Two numeric arrays and a constant are generated using the .txt to .MAT conversion program. The two arrays are a time array and amplitude array, where the time array spans the length of the recorded waveform and the amplitude array is the corresponding signal amplitude. The constant created by the conversion program is the sampling frequency of the digitizer, 2 GHz in this case. The time array is incremented over its span by $1/F_s$, 0.5 ns in this case, and the amplitude array contains the associated amplitude.

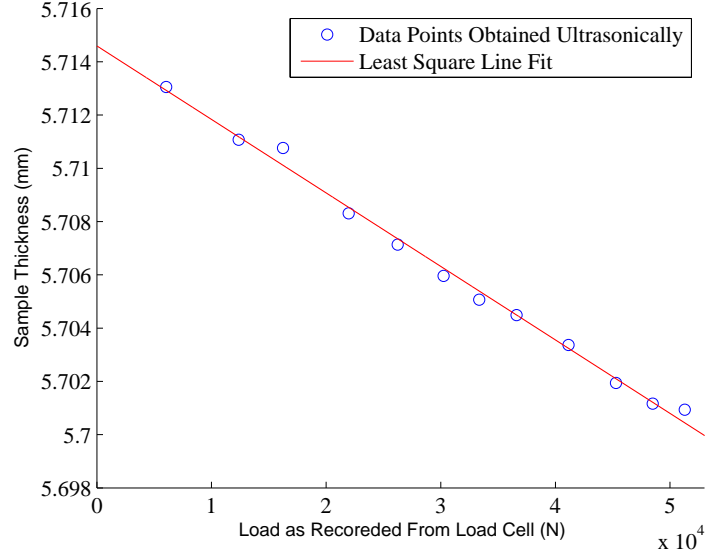


Figure 36: Typical Thickness vs Load Data: Longitudinal Wave

The first property to be measured is the sample thickness. The thickness can be determined by the relationship,

$$t = c_{L,water} \times [T_{tot} - \frac{1}{2}T_1 - \frac{1}{2}T_2] \quad (31)$$

in accordance with Fig. 16. Equation 31 is rearranged to Eq. 32.

$$t = \frac{1}{2}c_{L,water} \times [(T_{tot} - T_1) + (T_{tot} - T_1)] \quad (32)$$

Using Eq. 32 the differences can be determined using a cross correlation. This is accomplished with the “xcorr” function in MatLab with the water and front wall amplitude arrays. The cross correlation waveform is then transformed with a Hilbert transform and the data near the peak is curve fit with a second order polynomial to find it’s maximum, much in the way the normal angle was found in Section 2.2.2.1 (Fig. 19).

The loading array is generated manually. For each loading sequence the applied load is read from the digital “Panel Meter” and recorded with the corresponding waveforms.

The thickness and load are then plotted, a typical thickness versus load plot is shown in Fig. 36.

The TOF is calculated using the two pulses from the pulse echo waveform of transducer

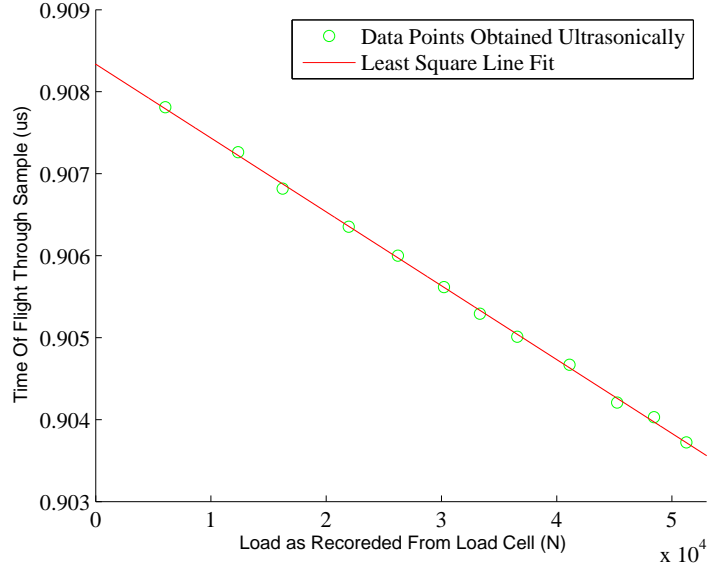


Figure 37: Typical TOF vs Load Data: Longitudinal Wave

1, Fig. 28. The TOF through the sample can be found by,

$$TOF_{AL} = \frac{1}{2}(T_{BackWall} - T_{FrontWall}) \quad (33)$$

The difference in Eq. 33 is found using the same cross correlating technique as the thickness calculation. The TOF and associated load are then plotted, a typical TOF versus load plot is shown in Fig. 37.

The velocity is calculated by dividing the thickness data by the TOF data, Eq. 28. The thickness and TOF are measured at the same incremental loadings therefore dividing the thickness array by the TOF array and plotting versus applied load yields the dependence of acoustic velocity on load, Fig. 38.

The acoustoelastic constant is found by taking the slope of the velocity stress curve and dividing by the initial velocity, Eq. 20. The applied load and the cross sectional area of the sample are used in order to determine the stress, Eq. 34.

$$\sigma = \frac{F}{A} \quad (34)$$

The velocity versus stress curve can now be plotted and the longitudinal acoustoelastic

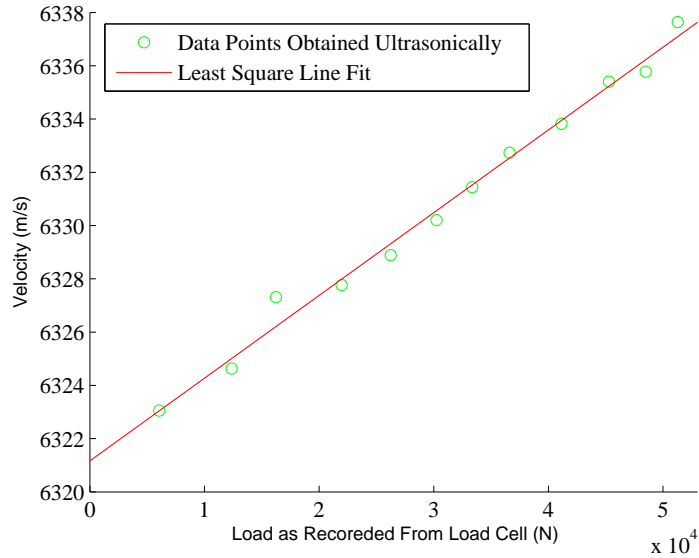


Figure 38: Typical Velocity vs Load Data: Longitudinal Wave

constant determined, a typical velocity versus stress plot is shown in Fig. 39.

3.1.2 Strain Mapping

A strain versus load profile was generated using all measured thickness versus load data. A strain versus stress profile was generated for all four samples prior to and after fatiguing, at three positions for each sample, and three repetitions at each position. The typical stress strain relationship for a given position is shown in Fig. 40.

A full presentation of the stress strain results and variation with sample and location is shown in the results section.

3.2 Contact Testing: Shear Acoustoelastic Constants

Ultrasonic pulse echo measurements, at various loads, are used to determine the horizontally and vertically polarized shear wave acoustoelastic constants. The pulse echo waveform is used to determine the TOF at a specific load. The load, read from the load cell display, is then used with the experimental stress strain relationship to determine the sample thickness. Using the TOF and thickness, the acoustic velocity is determined, Eq. 28. The acoustic velocity versus stress then yields the acoustoelastic constant for the shear wave of a specific

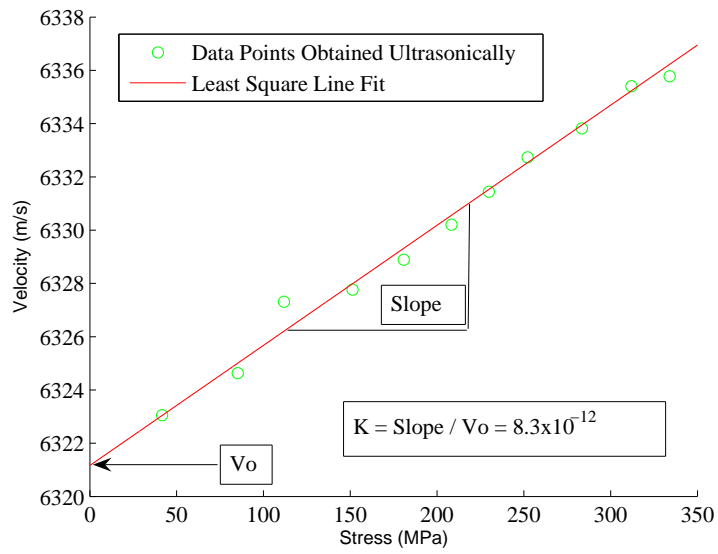


Figure 39: Typical Velocity vs Stress Data: Longitudinal Wave

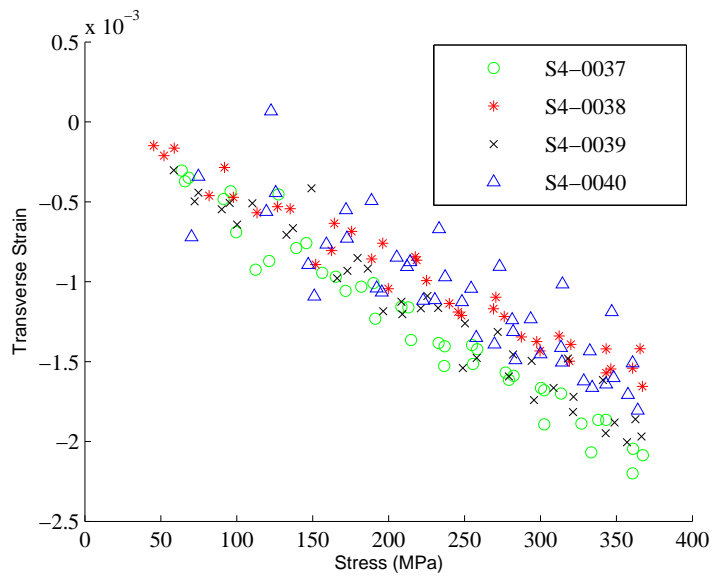


Figure 40: Typical Stress versus Strain Data

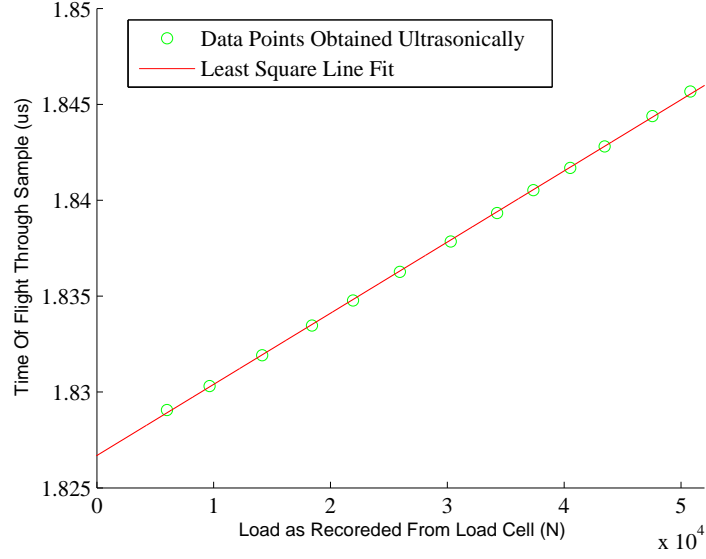


Figure 41: Typical TOF vs Load Data, Shear Wave

polarization, Eq. 20.

3.2.1 Shear Acoustoelastic Constants: TOF and Thickness

The time of flight versus load for a shear wave is determined using the pulse echo response. A typical pulse echo response contains two pulses, a front wall/couplant layer reflection and a back wall reflection, Fig. 32, a typical waveform is seen in Fig. 35.

The TOF, through the sample, is found by Eq. 35

$$TOF_{AL} = \frac{1}{2}(TOF_{BackWall} - TOF_{FrontWall/Couplant}) \quad (35)$$

The difference in Eq. 35 is found by cross correlating the two pulses in Fig. 35. This cross correlation is found by truncating the wave into two parts, each containing a pulse, and using the MatLab “xcorr” function. The cross correlation waveform is then transformed with a Hilbert transform and the data near the peak is curve fit with a second order polynomial to find it’s maximum, in the way the normal angle was found in Section 2.2.2.1 (Fig. 19). The TOF and associated load are then plotted, a typical TOF versus load plot is shown in Fig. 41.

The thickness, at a given load, is found using the stress strain relationship generated

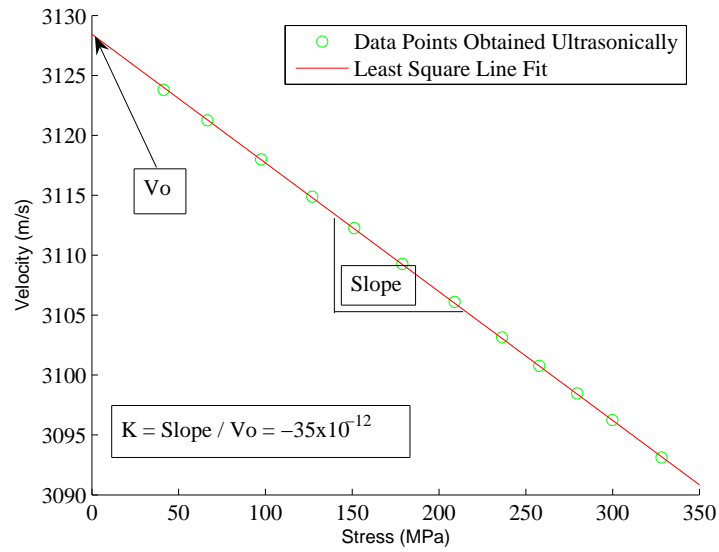


Figure 42: Typical Velocity vs Stress Data: Parallel Polarized Shear Wave

during longitudinal testing. This relationship was determined using every thickness versus load sequence. Each data sequence is linearly fit and the average of the coefficients is found. Using the averaged coefficients of these linear equations the thickness at any load can be found given the applied load.

The acoustoelastic constant is found by taking the slope of the velocity stress curve and dividing by the initial velocity, Eq. 33. The applied load and the cross sectional area of the sample is used in order to determine the stress, Eq. 34. The velocity versus stress curve can now be plotted and the shear acoustoelastic constants determined, a typical velocity versus stress plot is shown for parallel polarization in Fig. 42.

CHAPTER IV

RESULTS AND CONCLUSION

The previous chapters have outlined the physics and mathematics of the acoustoelastic constants, a series of experiments that were performed, and how the data from these experiments was analyzed. This chapter will present the results of all of the experimentation as well an interpretation of these results. Specifically, the acoustoelastic constants will be shown for longitudinal and shear waves. These values will be compared with literature values of similar materials, correlated with fatigue, and physically interpreted. Using these acoustoelastic constants the TOEC will be determined and mapped with damage. Further, for longitudinal immersion testing, strain results will be presented. To begin, however, the acoustoelastic constants will be decomposed and analyzed.

4.1 Decomposing the Acoustoelastic Constant: Density Effect and Elastic Nonlinearity

The following sections explore a decomposition of the acoustoelastic constant. The decomposition will no longer treat the second order elastic terms as strain invariant, specifically Young's modulus. This approach lends itself to physical interpretation of acoustoelasticity and shows how stress and wave orientation dictate the effect. Section 4.4 will use strain invariant second order elastic and third order elastic constants (TOEC).

The acoustic wave velocity is defined as,

$$c = \sqrt{\frac{\kappa}{\rho}} \quad (36)$$

where c is the phase velocity and κ is a combination of second order elastic constants, E and ν , Young's Modulus and Poisson's ratio, or λ and μ , the Lamé constants, and ρ is the density. The specific values for κ are shown in Eq. 37.

$$\kappa_L = \lambda + 2\mu \quad \kappa_S = \mu$$

$$\kappa_L = \frac{E(1-\nu)}{(1+\nu)(1-2\nu)} \quad \kappa_S = \frac{E}{2(1+\nu)} \quad (37)$$

The subscripts L and S in Eq. 37 represent longitudinal and shear waves, respectively.

Although this wave velocity is derived from the linearized wave equation, it can be used to explore nonlinearities by expanding for small perturbations at a fixed static stress, and no longer treating the elasticity or density as constants, Eq. 38.

$$\Delta c = \frac{1}{2} \frac{1}{\sqrt{\rho}} \frac{1}{\sqrt{\kappa}} \Delta \kappa - \frac{1}{2} \frac{\sqrt{\kappa}}{\rho \sqrt{\rho}} \Delta \rho \quad (38)$$

Dividing Eq. 38 by c and using the identity of c , Eq. 39 is obtained.

$$\frac{\Delta c}{c} = \frac{1}{2} \left[\frac{\Delta \kappa}{\kappa} - \frac{\Delta \rho}{\rho} \right] \quad (39)$$

A change in the wave velocity is governed by two terms, the density variation and the elastic variation.

Density Effect

First, we will look at how the density changes with stress. While elastically loading a specimen, it experiences a net change in volume. During this change in volume, the mass is conserved, thus yielding a change in density. A change in density will cause a change in the acoustic phase velocity, Eq. 39. This change in velocity is called the density effect.

Density is defined by,

$$\rho = \frac{M}{V} \quad (40)$$

where M is the mass and V is the volume. Expanding this identity for small perturbations gives Eq. 41.

$$\Delta \rho = \frac{1}{V} \Delta M - \frac{M}{V^2} \Delta V \quad (41)$$

Dividing by the density and using its identity yields Eq. 42.

$$\frac{\Delta \rho}{\rho} = \frac{\Delta M}{M} - \frac{\Delta V}{V} \quad (42)$$

The mass is constant, thus simplifying the expression to Eq. 43.

$$\frac{\Delta \rho}{\rho} = -\frac{\Delta V}{V} \quad (43)$$

Examining a control volume of our sample, the volume can be expressed using cartesian coordinates, x, y, z , as Eq. 44.

$$V = xyz \quad (44)$$

Small perturbations in the volume are expressed by Eq. 45.

$$\Delta V = yz\Delta x + xz\Delta y + xy\Delta z \quad (45)$$

Dividing Eq. 45 by the volume and using the identity for volume yields Eq. 46.

$$\frac{\Delta V}{V} = \frac{\Delta x}{x} + \frac{\Delta y}{y} + \frac{\Delta z}{z} \quad (46)$$

Using the definition of strain, Eq. 47,

$$\epsilon_i = \frac{\Delta i}{i} \quad i = x, y, z \quad (47)$$

the volume variation can be expressed as, Eq. 48.

$$\frac{\Delta V}{V} = \epsilon_x + \epsilon_y + \epsilon_z \quad (48)$$

For our specific case of uniaxial stress in the x direction (the selection of x is arbitrary), the strains are related through Hook's law by Eq. 49, where the transverse strains are assumed to be equal regardless of rolling orientation.

$$\begin{aligned} \epsilon_y &= -\nu\epsilon_x \\ \epsilon_z &= -\nu\epsilon_x \end{aligned} \quad (49)$$

Substituting these values into the volume variation, Eq. 46, in terms of ϵ_y (the strain in the thickness for our geometry) yields Eq. 50.

$$\frac{\Delta V}{V} = 2\epsilon_y - \frac{\epsilon_y}{\nu} \quad (50)$$

Substituting this relationship into the density variation relationship, Eq. 43, gives Eq. 51.

$$\frac{\Delta \rho}{\rho} = \frac{\epsilon_y}{\nu} - 2\epsilon_y \quad (51)$$

Substituting Eq. 51 into the velocity variation equation, Eq. 39, gives Eq. 52.

$$2\frac{\Delta c}{c} = \left[\frac{\Delta \kappa}{\kappa} - \left(\frac{\epsilon_y}{\nu} - 2\epsilon_y \right) \right] \quad (52)$$

All the quantities in this equation are known except for the elastic term κ and its variation, which have not been defined. The first term in Eq. 52 is the nonlinear contribution of the elasticity and the second term is the contribution from the density variation. Using Eq. 52 we can see how the density effect will contribute to the velocity variation.

Using the experimental results, shown in the following sections, for the velocity variation of a specified wave, Table 7 was generated for a fixed static stress of 350 MPa (the stress near peak loading). Table 7 outlines the contribution of the density effect to the velocity variation for each wave.

Table 7: Summary of the contribution from the density effect on the acoustoelastic constant at a static stress of 350 MPa.

	Shear Wave Parallel Stress	Shear Wave Perpendicular Stress	Longitudinal Wave Perpendicular Stress
$2\frac{\Delta c}{c}$	-24.12×10^{-3}	6.39×10^{-3}	5.92×10^{-3}
$-(\frac{\epsilon_y}{\nu} - 2\epsilon_y)$	1.62×10^{-3}	1.62×10^{-3}	1.62×10^{-3}
Density Effect	-6%	25%	27%

Table 7 shows that the density effect has less influence on the velocity variation than the elastic nonlinearity. The degree to which the density variation effects the nonlinearity depends on the magnitude of the acoustoelasticity, which is determined by the direction of the particle motion relative to the stress field.

For waves with particle motion normal to the tensile stress, the density effect accounts for about $\frac{1}{4}$ of the velocity increase.

The the density effect has little influence for waves with particle motion parallel to the applied stress. The negative percent indicates that the density effect is acting in opposition to the overall change in velocity. For the shear wave with particle motion parallel the stress, the density effect has essentially no contribution to the velocity change.

Elastic Nonlinearity

The specifics of the elastic variation are now explored. First, the elastic parameter, κ , is defined for longitudinal and shear waves using Young's modulus and Poisson's ratio, as in

Eq. 37, and are shown again in Eq. 53,

$$\kappa_L = \frac{E(1-\nu)}{(1+\nu)(1-2\nu)} \quad \kappa_S = \frac{E}{2(1+\nu)} \quad (53)$$

where the subscripts L and S are longitudinal and shear waves, respectively. Each elastic term can be expanded for small perturbations, Eq. 54.

$$\begin{aligned} \Delta\kappa_L &= \frac{(1-\nu)}{(1+\nu)(1-2\nu)}\Delta E - \frac{2\nu(\nu-2)E}{(\nu+1)^2(2\nu-1)^2}\Delta\nu \\ \Delta\kappa_S &= \frac{1}{2(1+\nu)}\Delta E - \frac{E}{2(\nu+1)^2}\Delta\nu \end{aligned} \quad (54)$$

Normalizing each perturbation in Eq. 54 and assuming Poisson's ratio to be constant gives Eq. 55.

$$\begin{aligned} \frac{\Delta\kappa_L}{\kappa_L} &= \frac{\Delta E}{E} \\ \frac{\Delta\kappa_S}{\kappa_S} &= \frac{\Delta E}{E} \end{aligned} \quad (55)$$

The elastic nonlinearity is now defined and the changes in the elasticity can be explored using the experimental values for the change in velocity and the strain in concordance with, Eq. 56.

$$2\frac{\Delta c}{c} = \left[\frac{\Delta E}{E} - \left(\frac{\epsilon_y}{\nu} - 2\epsilon_y \right) \right] \quad (56)$$

Table 8 shows the change in Young's modulus of elasticity.

Table 8: Summary of the change in elasticity and it's contribution to acoustoelasticity at a static stress of 350 MPa.

	Shear Wave Parallel Stress	Shear Wave Perpendicular Stress	Longitudinal Wave Perpendicular Stress
$2\frac{\Delta c}{c}$	-24.12×10^{-3}	6.39×10^{-3}	5.92×10^{-3}
$-\left(\frac{\epsilon_y}{\nu} - 2\epsilon_y\right)$	1.62×10^{-3}	1.62×10^{-3}	1.62×10^{-3}
$\frac{\Delta E}{E}$	-25.74×10^{-3}	4.77×10^{-3}	4.30×10^{-3}
Elastic Effect	+100%	75%	73%
Percent Change in Elasticity	2.6%	0.47%	0.43%

The trends, in terms of sign and magnitude of the change in elasticity, are in agreement with the model presented in Section 1.2.1 and Fig. 3. The disagreement between the perpendicular shear and longitudinal waves is within the experimental uncertainty. However the discrepancy could be due to the texture differences of rolled plate.

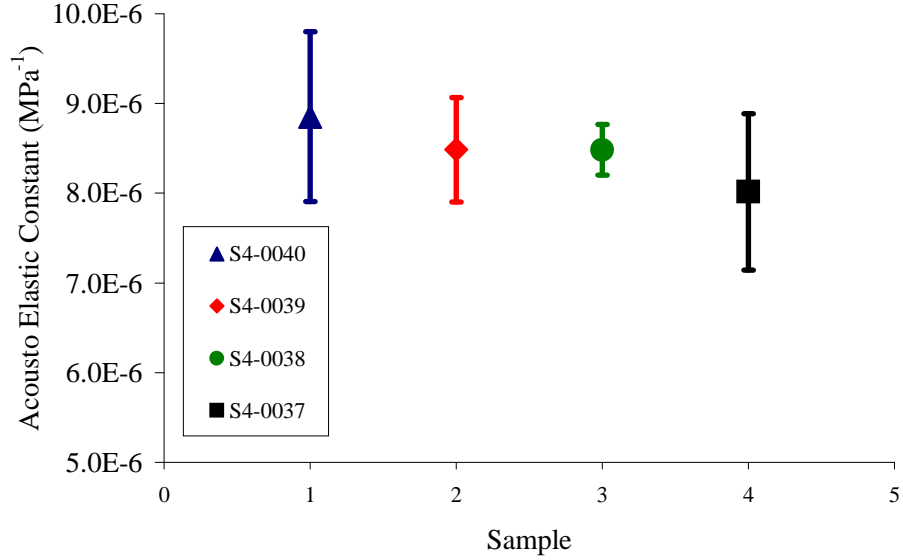


Figure 43: Acoustoelastic Constant for each Undamaged Sample: Longitudinal Wave Traveling Perpendicular to Loading

The percent change in elasticity is reasonable. Incrementing the applied static loading and calculating the change in elastic modulus, a table can be made showing the change in elasticity as a function of lattice strain, Appendix A. These values are a slope field for the binding force.

4.2 Longitudinal Testing: Results and Conclusions

For longitudinal immersion testing the acoustoelastic constant and strain mapping were measured and correlated with damage. The dependence of each of these parameters on sample inhomogeneity and fatigue life is explored within the experimental uncertainty.

4.2.1 Longitudinal Acoustoelastic Constant Results

The acoustoelastic constant for a longitudinal wave traveling perpendicular to uniaxial loading was measured for four samples before and after fatigue. For each sample the acoustoelastic constant is measured three times at three different locations along the gauge section.

The total average value of the acoustoelastic constant for each sample is shown in Fig. 43.

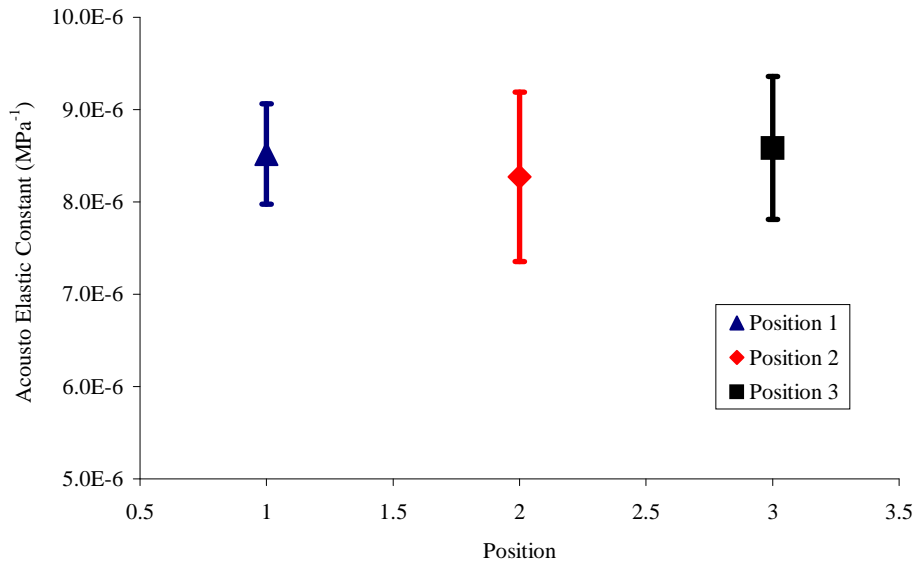


Figure 44: Acoustoelastic Constant for each Undamaged Position: Longitudinal Wave traveling perpendicular to applied uniaxial stress

The error bars in Fig. 43 represent one standard deviation in the repeated data. Examining Fig. 43, it is clear that each sample contains a fair amount of variance due to experimental error, about 8%. The results from sample to sample, however, are consistent within this uncertainty. Within the accuracy of this experiment there is no variation in the longitudinal acoustoelastic constant from sample to sample. This implies that the samples are comparatively homogenous, in terms of material composition and processing.

The average acoustoelastic constant is evaluated at three locations along the gauge section, Fig. 26, in order to further explore material homogeneity and the geometric dependence of the experiment. All three locations are completely in the gauge sections and should experience the same strain, therefore there should be no variation in the acoustoelastic constant. The average value of the acoustoelastic constant for each of the three locations is shown in Fig. 44.

Figure 44 shows the same experimental error that was seen from sample to sample, about 8%. The results for each location are consistent within the uncertainty. The agreement of the acoustoelastic constant along the gauge section implies the strain is truly uniform across the length of the gauge section, that was tested. Also, the material homogeneity and processing

is uniform along the gauge section, again, within uncertainty.

The variation in the acoustoelastic parameter is caused by experimental uncertainty due to system repeatability. This is explored in Section 4.5. The reported value for the acoustoelastic constant of 7075-T651 aluminum is therefore taken to be the average of the four undamaged samples. This value is shown in Table 9 along with some reported values from various literature sources for various aluminum treatments. The experimental value is in agreement with the reported values. Unfortunately no values for 7075-T6 AL were found.

Table 9: Summary of Acoustoelastic Constants for Longitudinal Waves Traveling Perpendicular to a Uniaxial Stress.

Acoustoelastic Constant MPa^{-1}	Material Type	Material Processing	Reference
$8.46 \pm 0.75 \times 10^{-6}$	AL 7075 – T651	Rolled Bar	Author
7.90×10^{-6}	AL 2024 – T3	Rolled Plate	[18]
8.90×10^{-6}	AL 2024 – T3	Rolled Plate	[18]
8.20×10^{-6}	AL Alloy 2214 – T6	Not Specified	[10]
13.50×10^{-6}	AL 2024 – T351	Rolled Sheet	[8]
7.4×10^{-6} (Rayleigh Wave)	AL Alloy 2214 – T6	Rolled Sheet	[6]

The longitudinal acoustoelastic constant, for AL 7075-T651, is in agreement with reported values for various aluminum alloys and tempers.

The acoustoelastic constant is also in agreement with the physical model developed in Section 1.2.1, as explained next.

The binding force curve in Fig. 3 and the velocity decomposition in Eq. 56 can be used to verify the acoustoelastic constant. For this experiment the wave particle motion is in a plane perpendicular to the load, hence the lattice strain, with respect to particle motion, is negative. This negative strain decreases the lattice spacing causing an increase in the interatomic repulsion which is proportional to elastic stiffness (Fig. 3). Transverse to stress, the elasticity increases with load, thus contributing to an increase in acoustic velocity.

The second term of the acoustic velocity is the density. Assuming conservation of mass, the density will decrease with loading, as discussed early. This decrease in density will

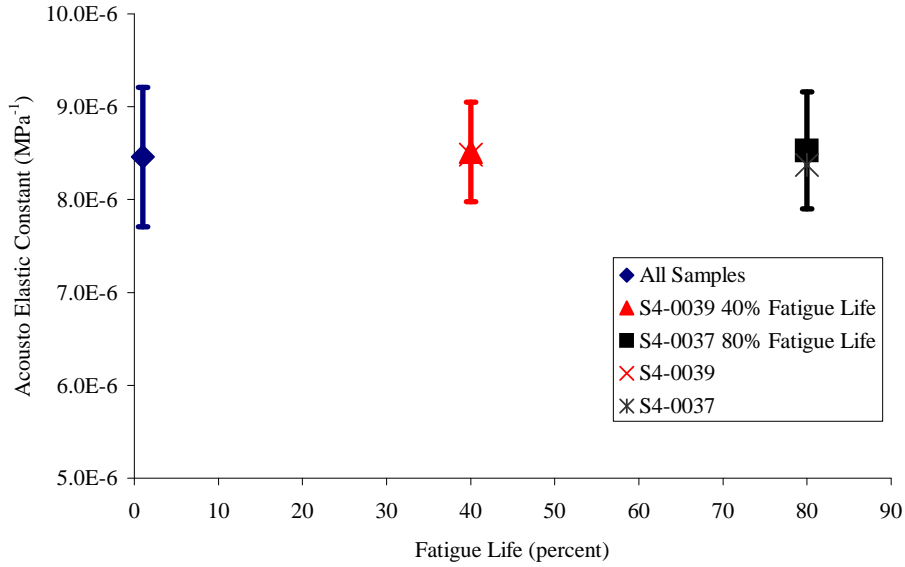


Figure 45: Acoustoelastic Constant for Damaged and Undamaged Samples: Longitudinal Wave Perpendicular to Loading

cause an increase in the velocity. Therefore in the case of wave motion perpendicular to loading the density and elastic nonlinearity effects work together to increase the acoustic phase velocity.

During fatiguing a specimen will experience several changes to its microstructure. The primary concern for this analysis is dislocation density and loop length. During the initial fatiguing the number and size of dislocations will increase substantially. Several models have been proposed to explain why acoustoelasticity should change during the fatigue process. One such model was presented in Eq. 21.

Figure 45 shows the total average acoustoelastic constant and that of two fatigue damaged samples. These results are also shown in Table 10.

Table 10: Summary of Acoustoelastic Constants for Longitudinal Waves Traveling Perpendicular to a Uniaxial Stress, undamaged and damaged.

Acoustoelastic Constant MPa^{-1}	Acoustoelastic Constant Damaged MPa^{-1}	
	All Samples	S4-0039 40% Fatigue Life
$8.46 \pm 0.75 \times 10^{-6}$	$8.53 \pm 0.65 \times 10^{-6}$	$8.61 \pm 0.48 \times 10^{-6}$

The results of the fatigued acoustoelastic constants shows some very promising trends

but are overall inconclusive. The results are inconclusive because there is essentially no variation in acoustoelasticity outside of the experimental uncertainty. This is not unexpected as the nonlinearity of aluminum is known to be small compared to other materials. Regardless, examining the average values several trends are present. First, the acoustoelasticity increases with fatigue damage. This increase is in concordance with the string model for dislocation damping, shown earlier. Another interesting trend, in terms of the average values, is the decrease in the rate of increasing acoustoelasticity. This is seen as the acoustoelastic percent increase from 0% to 40% fatigue life is greater than the percent increase from 40% to 80%. This result is as expected because the number of dislocations grows faster in the early stages of fatigue life as opposed to later stages. However, as mention before, the experiment is not precise enough to make any definite claims.

4.2.2 Strain Mapping Results

Thickness measurements were found at various uniaxial loads while finding the longitudinal acoustoelastic constants. These thickness measurements and load measurements are then used to generate a stress stain relationship. The stress strain relationship will give an external means for finding the sample thickness in the shear wave acoustoelastic constants calculation.

The strain transverse to loading direction is calculated using the definition of strain, Eq. 57.

$$\epsilon_y = \frac{\Delta y}{y} \quad (57)$$

The stress is determined using the applied load and the definition of stress, Eq. 58,

$$\sigma = \frac{F}{A} \quad (58)$$

where F is the applied force and A is the cross sectional area.

Using these definitions and the experimental data, stress strain plots were generated, Fig. 46. Figure 46 contains all of the stress strain data points for each sample.

Samples S4-0037 and S4-0040 are slightly offset from the other two samples, which fall nearly on top of each other. This is not a problem, however, as the slope of the stress strain curve is what is used.

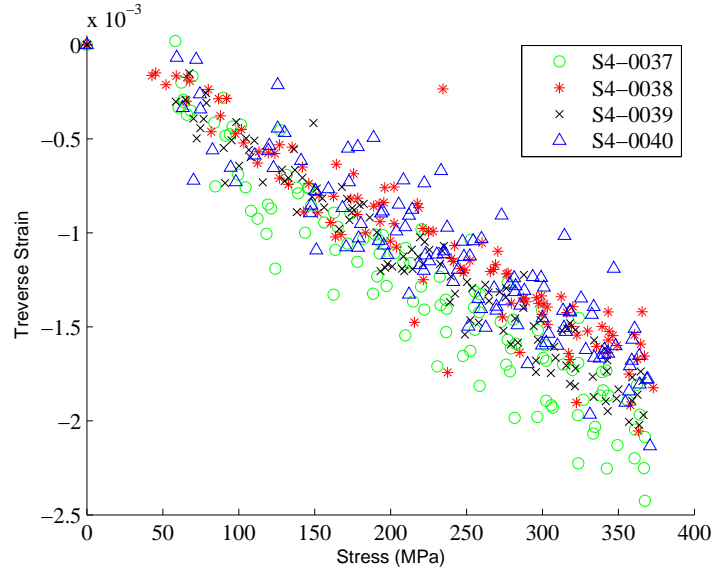


Figure 46: Stress versus Strain for each Specimen

Stress strain plots were also generated comparing the results as a function of position along the gauge section, Fig. 47.

The stress strain relationship is very similar as a function of sample position. The three location along the sample experience the same strain, within uncertainty.

The fatigued samples have also been analyzed in terms of stress and strain. The data, however, is offset from the series shown in Fig. 46. This offset is an artifact of the residual plastic deformation that occurs during fatigue damage. The slope of these stress strain curves is consistent with the undamaged samples. The vast majority of the microstructure still behaves elastically and thus this result is as expected.

A stress strain relationship was found using an average of the stress strain slopes of each sample at each location. All of the slopes are averaged as there is no stress strain dependence on sample or position. Using Poisson's ratio and the total stress strain slope, Young's modulus of elasticity can be determined for AL 7075-T651, Eq. 59.

$$E = -\nu \left(\frac{\sigma}{\epsilon_y} \right) \quad (59)$$

The slope of the various stress strain curves and values of Young's Modulus are found in Tables 11, 12, and 13.

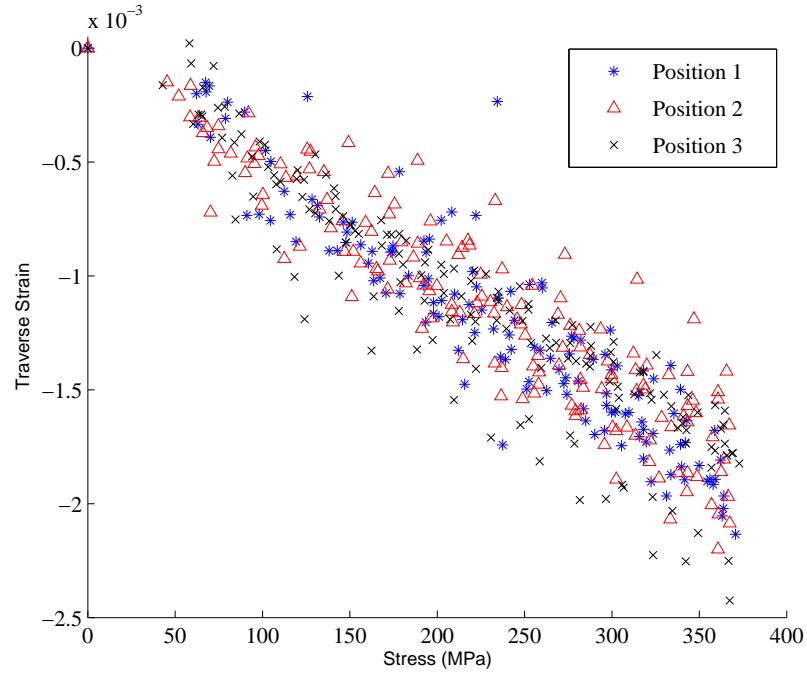


Figure 47: Stress versus Strain for each Location

Table 11: Young’s Modulus Table Value Versus Experimental Value

Young’s Modulus, E (GPa)	
Table Value [9]	Total Average Experimental Value
AL 7075-T6	AL 7075-T651
71.00	67.56 ± 1.50

The experimental value calculated for Young’s Modulus is less than the literature value for a similar temper. This discrepancy may be due to the intrinsic differences due to material processing. The experimental value was determined measuring the transverse strain on a rolled sample where as the literature value uses untreated material.

Tables 12 and 13 show the slope of the stress strain curve grouped by gauge section position and sample, respectively. The position grouped values are equal within uncertainty, implying a uniform stress strain relation along the gauge section. The sample grouped values are equal within uncertainty, implying uniform stress strain from sample to sample.

Table 12: Stress Strain Relationship For Various Positions

Slope Stress Strain Curve, $\Delta\epsilon/\Delta\sigma$ (MPa^{-1})		
Position 1	Position 2	Position 3
$-5.10 \pm 0.372 \times 10^{-6}$	$-4.99 \pm 0.708 \times 10^{-6}$	$-5.19 \pm 0.798 \times 10^{-6}$

Table 13: Stress Strain Relationship For Various Samples

Slope Stress Strain Curve, $\Delta\epsilon/\Delta\sigma$ (MPa^{-1})			
S4-0037	S4-0038	S4-0039	S4-0040
$-5.46 \pm 0.451 \times 10^{-6}$	$-4.70 \pm 0.324 \times 10^{-6}$	$-5.20 \pm 0.354 \times 10^{-6}$	$-4.73 \pm 0.506 \times 10^{-6}$

4.3 Results for Contacting Testing: Shear Acoustoelastic Constants

For contact testing one parameter is measured and correlated with damage, the acoustoelastic constant. The dependence of this parameter on sample inhomogeneity and fatigue life is explored within the experimental uncertainty. The values for the two polarized acoustoelastic constants are compared with reported values and correlated to the physical models.

The acoustoelastic constants for shear waves traveling perpendicular to uniaxial loading with particle motion perpendicular and parallel to the loading is measured for one undamaged sample (S4-0040) and for two fatigued samples (S4-0037 and S4-0039). For each sample the acoustoelastic constant is measured three times at three different locations along the gauge section.

Shear Acoustoelastic Constant Particle Motion Perpendicular Stress

The acoustoelastic constant for shear waves traveling perpendicular to the loading with particle motion perpendicular the loading is shown in Fig. 48.

The value obtained for the perpendicular shear acoustoelastic constant is as expected in terms of magnitude and sign, $8 - 10 \times 10^{-12}$ and positive. This value is in agreement with reported values for similar materials, Table 14.

Also the perpendicular shear acoustoelastic constant is close to the longitudinal acoustoelastic constant found in Section 4.2.1. This should be the case as both waves have particle

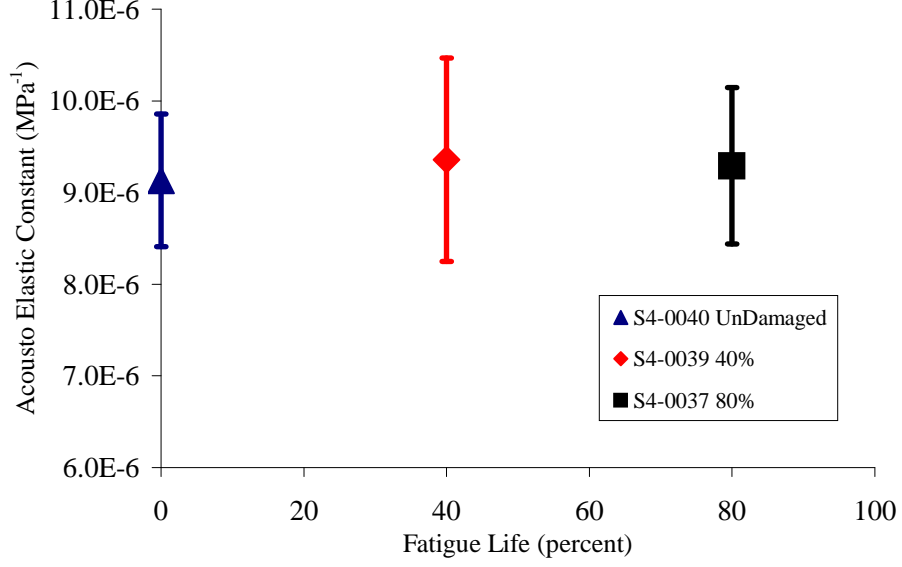


Figure 48: Acoustoelastic Constant for Damaged and Undamaged Samples: Shear Wave Traveling Perpendicular to Uniaxial Stress with Particle Motion Perpendicular to Uniaxial Stress

Table 14: Summary of Acoustoelastic Constants for Shear Wave Traveling Perpendicular to Uniaxial Stress with Particle Motion Perpendicular to Uniaxial Stress.

Acoustoelastic Constant MPa^{-1}	Material Type	Material Processing	Reference
$9.13 \pm 0.72 \times 10^{-6}$	AL 7075 – T6	Rolled Bar	Author
7.30×10^{-6}	AL Alloy 2214 – T6	Not Specified	[10]
10.60×10^{-6}	AL 2024 – T351	Rolled Sheet	[8]

motion and propagation direction perpendicular to the loading. As discussed earlier in Section 4.1, the lattice plane transverse the loading direction will become increasingly rigid with stress, causing an increase in elasticity. The longitudinal and shear acoustoelastic constants should not be identical, however, as the particle motion with respect to the propagation is different and the particle propagation mechanics are different.

Mapping the perpendicular polarized acoustoelastic constant with fatigue damaged showed promising trends but was inconclusive, as was the case for the longitudinal wave. There is a small increase in acoustoelasticity with fatigue damage. This increase is explained using the dislocation model presented earlier in Section 1.2.2. The change is, however, not

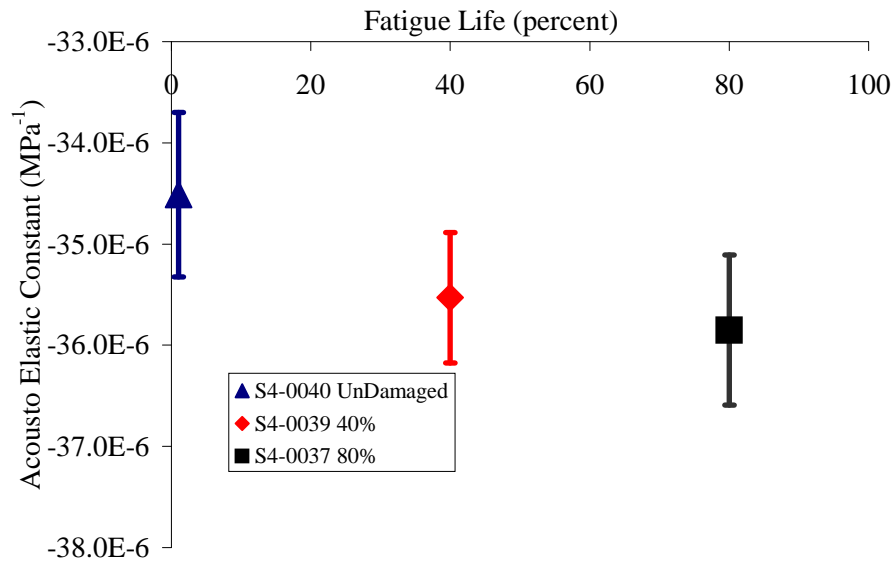


Figure 49: Acoustoelastic Constant for Damaged and Undamaged Samples: Shear Waves Traveling Perpendicular to a Uniaxial Stress with Particle Motion Parallel to a Uniaxial Stress

outside the experimental uncertainty.

Shear Acoustoelastic Constant Particle Motion Parallel Stress

The acoustoelastic constant for shear waves traveling perpendicular to the loading with particle motion parallel the loading is shown in Fig. 49.

The value obtained for the parallel shear acoustoelastic constant is as expected in terms of magnitude and sign. This value is in agreement with reported values for similar materials, Table 15.

The sign of the acoustoelastic constant changes due to the change in polarization with respect to the loading. The shear wave is now polarized such that the particle motion is in the direction of positive strain. The positive strain causes the lattice to elongate. The nonlinearity with increasing interatomic separation has a relaxing effect on the elasticity according to the model in Fig. 3. A relaxing, or decreasing in magnitude, elasticity will cause a decrease in acoustic phase velocity.

Table 15: Summary of Acoustoelastic Constants for Shear Waves Traveling Perpendicular to a Uniaxial Stress with Particle Motion Parallel to a Uniaxial Stress.

Acoustoelastic Constant MPa^{-1}	Material Type	Material Processing	Reference
$-34.45 \pm 0.81 \times 10^{-6}$	<i>AL 7075 – T651</i>	<i>Rolled Bar</i>	Author
$-35.53 \pm 0.64 \times 10^{-6}$	<i>AL 7075 – T651 40% Life</i>	<i>Rolled Bar</i>	Author
$-35.85 \pm 0.74 \times 10^{-6}$	<i>AL 7075 – T651 80% Life</i>	<i>Rolled Bar</i>	Author
-33.50×10^{-6}	<i>AL Alloy 2214 – T6</i>	<i>Not Specified</i>	[10]
-29.70×10^{-6}	<i>AL 2024 – T351</i>	<i>Rolled Sheet</i>	[8]

Another very interesting feature is the increased magnitude of the acoustoelastic constant, with respect to the perpendicularly polarized wave. The parallel wave is about 4 times that of the perpendicular wave.

The density effect will increase wave speed regardless of polarization. Although the density effect is smaller than the elastic nonlinearity it's opposition to the net change only serves to bolster the disparity in nonlinearity with respect to lattice strain orientation.

The larger magnitude of the parallel acoustoelasticity is explained by the increased strain in the direction of loading and the potential well model in Fig. 3. The strain parallel the loading is larger than the strain perpendicular the loading, this increased strain causes larger lattice separation and hence a larger change in elasticity. However, even at equal strains the parallel acoustoelasticity is larger. This increase in acoustoelasticity is due to the increased nonlinearity in the binding energy curve with lattice elongation, Fig. 3 [2].

Mapping the acoustoelastic constant for shear waves with particle polarization parallel applied stress versus fatigue damaged shows very promising trends and should be further investigated. The acoustoelasticity increases in magnitude with increasing damage. This correlation is as expected following the dislocation model, Eq. 21.

The absolute change in acoustoelasticity was much larger for the parallel wave. This may suggest that the dislocation model is directionally dependent. However, if the percent change in the acoustoelastic constant is used the directionality is less apparent, Table 16. The current model does not give directional dependence or percent changes.

Table 16: Changes of Acoustoelastic Constants with Damage for Shear Waves

	Parallel	Perpendicular
Base Value	$-34.45 \times 10^{-6} \text{ MPa}^{-1}$	$9.13 \times 10^{-6} \text{ MPa}^{-1}$
Change With Damage (80% Life)	$-1.400 \times 10^{-6} \text{ MPa}^{-1}$	$0.225 \times 10^{-6} \text{ MPa}^{-1}$
Percent Change	4.0%	2.5%

Another positive trend, in terms of a dislocation model, is the decreasing rate of acoustoelastic variation with damage. The majority of dislocation are formed in the initial stages of fatigue damage, as discussed earlier. During latter stages of fatigue, dislocation tend to “pile up” and interact with each other as opposed to strictly increase in number. Following this logic and the dislocation model, the change in acoustoelasticity should be greater during the first 0% to 40% of life than for the later 40% to 80% of life, and it is, Table 17.

Table 17: Changes of Acoustoelastic Constants with Damage for Shear Waves Traveling Perpendicular to a Uniaxial Stress with Particle Motion Parallel to a Uniaxial Stress

	0% to 40% Life	40% to 80% Life
Base Value	$-34.45 \times 10^{-6} \text{ MPa}^{-1}$	$-35.53 \times 10^{-6} \text{ MPa}^{-1}$
Change With Damage	$-1.080 \times 10^{-6} \text{ MPa}^{-1}$	$-0.318 \times 10^{-6} \text{ MPa}^{-1}$
Percent Change	3.1%	0.9%

The trend with fatigue damage is much more apparent in this case than either of the particle motion perpendicular load waves. The trend is still near the limit of experimental uncertainty, therefore, further testing should be performed in order to verify and explore these results.

4.4 Third Order Elastic Constants For 7075-T651 Aluminum and Their Variation with Damage

At the beginning of the results section an analysis was performed in which the second order elastic constant, Young’s Modulus, was no longer treated as stress invariant. This treatment was made in concordance with the physics model of material nonlinearity in which the elasticity is dependent on stress. However, a more common approach to acoustoelasticity and material nonlinearity is keeping the second order elastic properties constant, with stress,

and adding third order elastic terms (TOEC). The following section computes these third order constants for 7075-T651 aluminum. Further, these constants are then mapped with fatigue damage, as the acoustoelastic constants were.

The acoustoelasticity was defined in terms of third order elastic constants in Section 1.2.2. The values for these third order elastic constants were ignored at the time because an acoustoelastic constant was adapted instead. The following uses these acoustoelastic constants to determine the TOEC.

Using the stress dependent velocity derivation in Section 1.2.2, three acoustic waves can be defined. The velocity, $c_{1,2,3}$, will be defined as such: the first subscript will denote the wave type with l for longitudinal and s for shear, the second subscript will denote the propagation direction where n indicates the direction normal to the applied uniaxial stress, and the third subscript will denote the particle polarization where n indicates particle motion normal, perpendicular, to the applied stress and p denotes particle motion parallel to the applied stress (for longitudinal waves the particle motion is in the same direction as the propagation thus just two indices are used). Using this nomenclature, the acoustic velocities can be written in terms of the applied tensile stress, σ , and the second and third order elastic constants, Eq. 60.

$$\begin{aligned}
\rho c_{l,n}^2 &= \lambda + 2\mu + \frac{\sigma}{3\lambda + 2\mu} \left[2l - \frac{2\lambda}{\mu} (m + \lambda + 2\mu) \right] \\
\rho c_{s,n,p}^2 &= \mu + \frac{\sigma}{3\lambda + 2\mu} \left(m + \frac{\lambda n}{4\mu} + \lambda + 2\mu \right) \\
\rho c_{s,n,n}^2 &= \mu + \frac{\sigma}{3\lambda + 2\mu} \left(m - \frac{\lambda + \mu}{2\mu} n - 2\lambda \right)
\end{aligned} \tag{60}$$

These three linear independent equations can be solved for the three unknowns, l, m, n , the Murnaghan constants.

To begin, several substitutions can be made to simplify the algebra.

$$\begin{aligned}
A &= \frac{\sigma}{3\lambda + 2\mu} \\
B &= \lambda + 2\mu \\
C &= \frac{\lambda + \mu}{2\mu} \\
D &= \frac{\lambda}{\mu}
\end{aligned} \tag{61}$$

Using these substitutions the velocity equations can be written as Eq (62).

$$\begin{aligned}
\rho c_{l,n}^2 &= B + A[2l - 2D(m + B)] \\
\rho c_{s,n,p}^2 &= \mu + A(m + \frac{1}{4}Dn + B) \\
\rho c_{s,n,n}^2 &= \mu + A(m - Cn - 2\lambda)
\end{aligned} \tag{62}$$

Subtracting the two shear equations yields one equation in terms of n , Eq. 63.

$$(\rho c_{s,n,p}^2 - \rho c_{s,n,n}^2) = A(\frac{1}{4}D + C)n + A(B + 2\lambda) \tag{63}$$

Solving this equation for n yields Eq. 64.

$$n = \frac{[(\rho c_{s,n,p}^2 - \rho c_{s,n,n}^2) - A(B + 2\lambda)]}{A(\frac{1}{4}D + C)} \tag{64}$$

With n determined, m can be solved using either shear equation, using the $c_{s,n,n}$ velocity, m can be solved with Eq. 65.

$$m = \frac{1}{A} [\rho c_{s,n,n}^2 - \mu + ACn + 2\lambda A] \tag{65}$$

Now that m has been determined, l can be solved using the longitudinal velocity Eq. 66.

$$l = \frac{1}{2} \left[\frac{\rho c_{l,n}^2}{A} - \frac{B}{A} + 2D(m + B) \right] \tag{66}$$

Using a uniaxial stress of 350 MPa and the appropriate velocities, as determined using the acoustoelastic constants, the third order elastic constants can be determined and are found in the following Table 18.

Table 18: Second and Third Order Elastic Constants for 7075-T651 Aluminium

λ	μ	l	m	n
10^{10} N/m^2	10^{10} N/m^2	10^{10} N/m^2	10^{10} N/m^2	10^{10} N/m^2
5.49	2.65	-25.22	-32.50	-35.12

Using the TOEC and the velocity equations, developed in Section 1.2.2, the acoustic velocity in stressed 7075 aluminum can be determined. The next chapter will show an application of how the TOEC can be used to solve a “real world” problem.

Table 19: Third Order Elastic Constants for 7075-T651 Aluminium at Different Levels of Fatigue Damage

Fatigue Life	l	m	n
Percent Life	$10^{10} N/m^2$	$10^{10} N/m^2$	$10^{10} N/m^2$
0%	-25.22	-32.50	-35.12
40%	-26.68	-33.28	-35.83
80%	-27.12	-33.58	-35.98

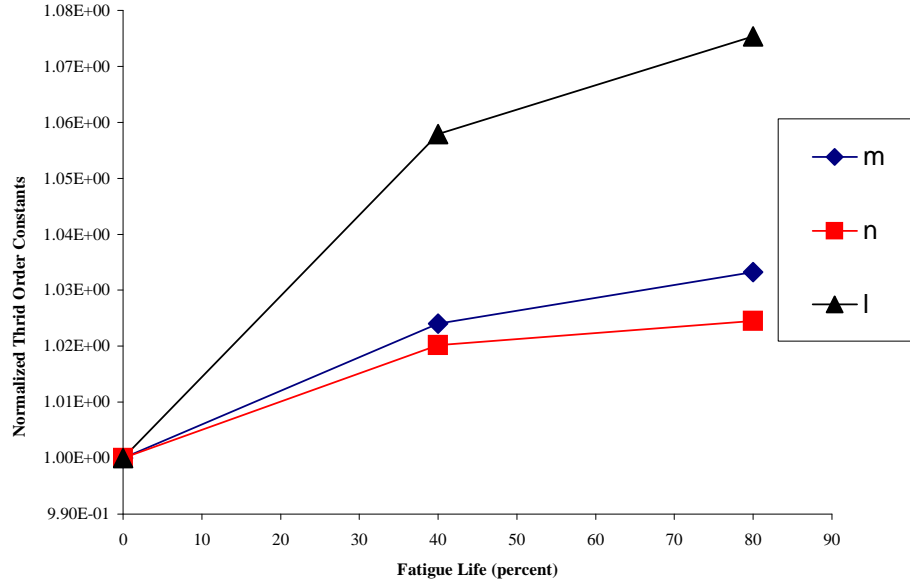


Figure 50: TOEC for Damaged and Undamaged Samples

Another possible application of the TOEC is using them as a damage detection parameter. Using the acoustoelastic constants for the fatigued samples, the TOEC can be recalculated. Table 19 shows the TOEC constants variation with damage.

There is certainly a trend in the third order elastic constants with damage. This trend should be expected, however, as all three acoustoelastic constants showed a trend with damage and the TOEC are computed using the acoustoelastic constants.

In order to explore the relative sensitivity in the TOEC, each constant is normalized to the undamaged value and plotted versus fatigue life, Fig. 50.

The normalized TOEC versus fatigue life in Fig. 50 show a trend with damage. Further,

it appears that the l TOEC is more sensitive to damage than the m or n . The l parameter is only found in the longitudinal velocity equations. This result seems peculiar as the longitudinal acoustoelastic constant was not more sensitive than the shear acoustoelastic constants.

Another trend in Fig. 50, is the decreasing rate of change in the TOEC with damage. This is in agreement with the dislocation model developed earlier. The damage mechanisms which effect acoustoelasticity are more prevalent in the earlier stages of fatigue damage than the later stages.

The TOEC show the same trend with damage as the acoustoelastic constants. Whether the TOEC can be used to detect fatigue damage and if any one of these parameters is more sensitive or a better indicator of fatigue damage should be further explored.

4.5 Uncertainty and Error Propagation

A great deal of this paper outlined the experimental and computational techniques for determining the various acoustoelastic, third order elastic, properties of 7075 aluminum. These techniques were outlined and described in such detail because acoustoelasticity is a very small effect. Further, in order to correlate this already small effect with damage, a high degree of experimental accuracy is required. As such, the following section will detail the propagation of the allowed strain uncertainty, described in Section 2.2.2.2. This uncertainty will be carried through one calculation of two acoustoelastic constants and compared with the statistical error found in the experimental data.

The maximum allowable strain error, as detailed in in Section 2.2.2.2, is 10%. For the purpose of this exercise we will consider this to be the only experimental uncertainty.

To begin, the average transverse strain at 350 *MPa* is,

$$\epsilon = \frac{\Delta L}{L} = 1.783 \times 10^{-3} \quad (67)$$

where L is the thickness of the sample, as was found in Table 12. Now, the 10% uncertainty is added and the strain is multiplied by the initial thickness, which we will assume to be exactly 5.71 *mm*. This will allow us define the thickness at initial and final stress including

the strain uncertainty, Eq 68.

$$\begin{aligned}\frac{\Delta L}{L} &= 1.783 \pm 0.178 \times 10^{-3} \\ \Delta L &= 10.181 \pm 1.018 \times 10^{-3} \text{ mm} \\ L_{0MPa} &= 5.71 \text{ mm} \\ L_{350MPa} &= 5.699820 \pm 0.001018 \text{ mm}\end{aligned}\tag{68}$$

This is the strain error uncertainty that will be propagated through the calculation of the acoustoelastic constants.

Equation 69 will be used to calculate the acoustoelastic constants,

$$K = \frac{1}{350 \text{ MPa}} \times \frac{1}{c_{0MPa}} \times \left[\frac{L_{350 \text{ MPa}}}{T_{350MPa}} - \frac{L_{0MPa}}{T_{0MPa}} \right]\tag{69}$$

where the T 's are the time of flight at the given static load. The TOF's will be taken from actual data. The TOF's and stress will be assumed to have no uncertainty.

The step by step results for Eq 69. with uncertainty for two acoustic wave types is shown in Tables 20 and 21.

Table 20: Strain Uncertainty Propagation to the Acoustoelastic Constant for Shear Wave Polarized with Particle Motion Parallel Stress

Shear Wave Particle Polarization Parallel Stress			
Equation Step	Value	Uncertainty	Percent
$\frac{L_{350MPa}}{T_{350MPa}}$	3092.31 m/s	$\pm 0.55 \text{ m/s}$	$\pm 0.02\%$
" - $\frac{L_{0MPa}}{T_{0MPa}}$	-37.685 m/s	$\pm 0.55 \text{ m/s}$	$\pm 1.5\%$
" $\times \frac{1}{c_{0MPa}}$	-12.04^{-3}	$\pm 0.18^{-3}$	$\pm 1.5\%$
" $\times \frac{1}{350 \text{ MPa}} = K$	-34.40 MPa^{-1}	$\pm 0.51 \text{ MPa}^{-1}$	$\pm 1.5\%$
Experimental K	-34.45 MPa^{-1}	$\pm 0.81 \text{ MPa}^{-1}$	$\pm 2.3\%$

The results in Tables 20 and 21 show how the strain uncertainty propagates to the acoustoelastic constant. The lines entitled horizontal K show the experimentally determined values for K and an associated uncertainty based on one standard deviation in the data.

One inference that can be made from this analysis is that the strain uncertainty accounts for most of the scatter in the data. The statistical variation is close to what would occur if the only uncertainty was the strain and a series of measurements were taken.

Table 21: Strain Uncertainty Propagation to the Acoustoelastic Constant for Longitudinal Wave

Longitudinal Wave			
Equation Step	Value	Uncertainty	Percent
$\frac{L_{350MPa}}{T_{350MPa}}$	6339.61 <i>m/s</i>	± 1.13 <i>m/s</i>	$\pm 0.02\%$
" - $\frac{L_{0MPa}}{T_{0MPa}}$	19.61 <i>m/s</i>	± 1.13 <i>m/s</i>	$\pm 5.8\%$
" $\times \frac{1}{c_{0MPa}}$	3.10^{-3}	$\pm 0.18^{-3}$	$\pm 5.8\%$
" $\times \frac{1}{350 MPa} = K$	8.80 <i>MPa</i> ⁻¹	± 0.51 <i>MPa</i> ⁻¹	$\pm 5.8\%$
Experimental K	8.46 <i>MPa</i> ⁻¹	± 0.75 <i>MPa</i> ⁻¹	$\pm 8.8\%$

In this calculation, the TOF measurements were considered to have no uncertainty. However, in reality the TOF measurements experience much of the same uncertainty as the strain measurements.

Another interesting observation is how the relative strain error effects different acoustoelastic constants. In the results section it was shown that only the shear wave polarized with particle motion parallel loading could show a trend with damage, outside uncertainty. This may be due to the magnitude of the nonlinear effect relative to the uncertainty not because the shear wave polarized parallel strain is more sensitive to damage than the other waves. Tables 20 and 21 show how the absolute strain uncertainty is the same for each wave, but the percent error is dependent on the magnitude of the acoustoelastic constant.

CHAPTER V

APPLICATION OF TOEC

In this work, acoustoelasticity and the TOEC have been treated in a very theoretical manner in terms of their presence and application. The following chapter will outline a practical ultrasonic application in which knowledge of TOEC is required. The presented example has been taken from a real research project at Georgia Institute of Technology [17] funded through DARPA. Actual data from this project will be shown and explained using the TOEC from this paper. This example will show how acoustoelasticity plays a roll in ultrasonic testing and will serve as further validation of the TOEC computed in this paper.

The researchers, in this case, were concerned with dynamically determining the uniaxial applied stress on a sample of 7075-T651 aluminum. The experimental setup has two 70° angle beam transducers mounted on the surface of the sample Fig. 51.

The receiving transducer receives two distinct pulses representing the wave paths labeled “Single V” and “Double V” in Fig. 51. These pulses can be seen in Fig. 52. When a uniaxial stress is applied to the sample the TOF for these pulses will change, Fig. 52.

The change in TOF, with applied static loading, is due to two effects. The first being, the wave path changes under elastic loading, geometry effect. The second is the acoustic wave speed changes due to the acoustoelastic effect.

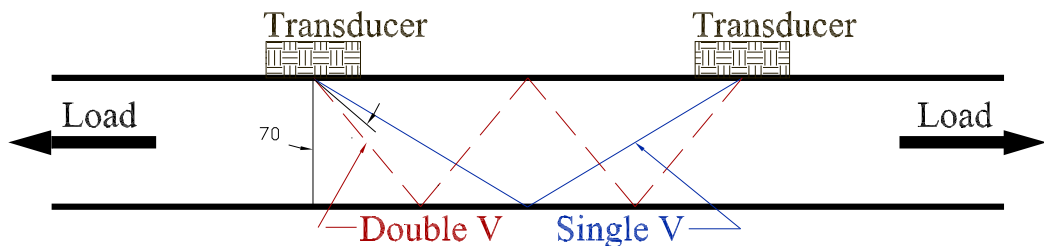


Figure 51: Shear Transducer Geometric Setup

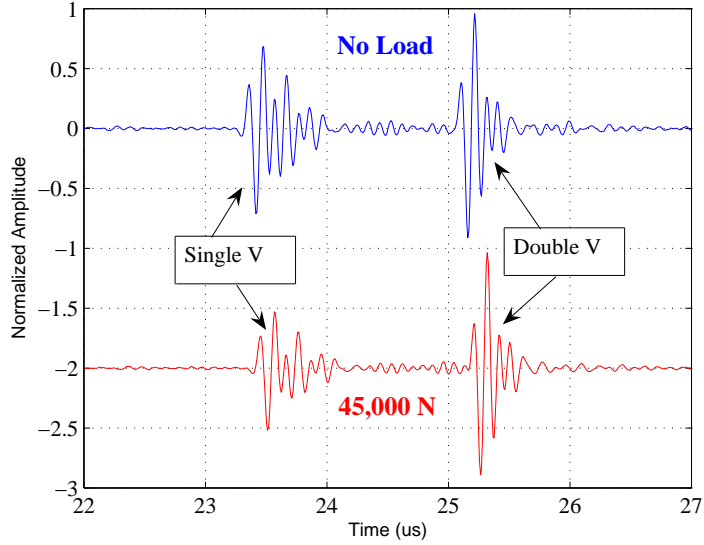


Figure 52: Example Waveform Showing Two Pulses Representing The Single And Double V Wave Paths and TOF Shift With Load

The geometric effect can be determined using Hooke’s law and tabular values for the elastic constants or by using strain gauges. Regardless, the geometry of the “Single V” and “Double V” paths as functions of stress can be analytically calculated.

Now, using the stress dependent acoustic velocity equations, the third order elastic constants, Eq. 19, and measuring the TOF, the applied static load can be determined.

It should be noted that the stress dependent acoustic velocity expressions in Eq. 19 do not describe shear wave motion at an angle to an applied loading. However, using a coordinate system transformation and re-deriving the velocity equations it is possible to describe the angular shear velocity, as a function of stress, with two second order elastic constants and three third order elastic constants. This derivation is not shown here but can be found in reference [17]. Using the third order elastic constants, calculated in this paper, and the geometry effect, a theoretical change in TOF versus applied static loading curve is generated and compared to experimental data, Fig. 53 [17].

Figure 53 shows an excellent agreement between the theoretical values and experimental data. Using the TOEC the researchers are able to determine the local applied stress on the sample by recording the TOF between the two transducers.

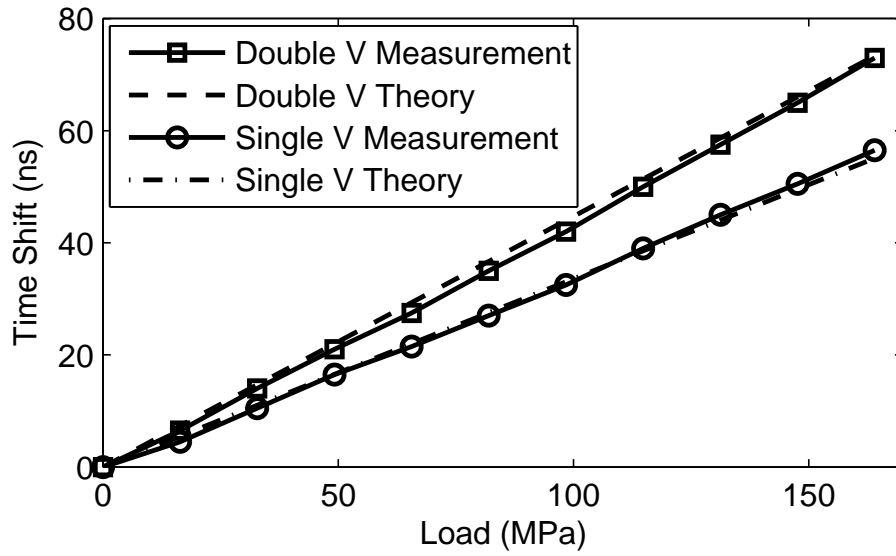


Figure 53: Experimental TOF Data Versus Theoretical TOF.

This example shows one possible application of TOEC and describes an ultrasonic experiment in which acoustoelasticity plays an integral role. Further, this example serves to bolster the validity of the TOEC (acoustoelastic constants) values presented.

CHAPTER VI

CONCLUSIONS AND RECOMMENDATIONS

The acoustoelastic constants, in terms of Eq. 20, have been calculated for a longitudinal wave traveling perpendicular to a uniaxial stress, a shear wave traveling perpendicular a uniaxial stress with particle motion polarized perpendicular the stress, and a shear wave traveling perpendicular a uniaxial stress with particle motion polarized parallel the stress in AL 7075-T651. The experimental values for the acoustoelastic constants are in agreement with reported values for similar aluminum alloys.

The acoustoelasticity increases with fatigue damage due to the presence of dislocations. The change in acoustoelasticity with damage, for waves with particle motion perpendicular to stress, could not be confirmed due to experimental uncertainty. Shear waves, polarized with particle motion parallel to stress, showed promise for fatigue damage detection. The primary advantage of the in line stress polarization, is the increased magnitude of the acoustoelastic constant and the increase in change with damage. Future work should be performed to reduce experimental error and create more data in order to explore acoustoelasticity as a function of fatigue life.

Using the acoustoelastic constants the third order elastic constants were calculated for 7075-T651 aluminium. An application showed how the TOEC could be used to deduce the uniaxial load from shear angle beam TOF measurements. This application of the TOEC reinforced their validity and displayed their usefulness in precision ultrasonic work.

The TOEC showed a trend with fatigue damage. Using the Murnaghan definition for the TOEC, the l parameter showed the greatest change with fatigue damage. As with using the acoustoelastic constants, future work should be performed to reduce experimental error and create more data in order to explore TOEC as a function of fatigue life.

Pulse echo scanning in an immersion tank provides a sensitive and reliable technique for non contact thickness measurements. This technique is nothing new in terms of ultrasonic

testing, but the strain mapping procedure does outline a number a limitations and difficulties in performing high accuracy thickness measurements.

In closing, nonlinear ultrasonics provides a number of exciting tools for qualitative non-destructive testing. For some materials changes in TOEC may be a useful indicator of damage. For 7075-T651 aluminum, which has a very small nonlinear effect, the TOEC changes are small and difficult to measure accurately enough to track damage.

APPENDIX A

CHANGE IN ELASTICITY AS A FUNCTION OF STRAIN

The change in Young's Modulus as a function of strain was explored in Section 4.1. The following appendix will further explore this relationship for shear waves traveling parallel and perpendicular to an applied uniaxial stress.

Starting with Eq. 52,

$$2\frac{\Delta c}{c} = \left[\frac{\Delta E}{E} - \left(\frac{\epsilon_x}{\nu} - 2\epsilon_x \right) \right]$$

and using the linear acoustoelastic definition, Eq. 20,

$$\frac{\Delta c}{c_o} = K \Delta \sigma$$

Eq. 52 can be written in terms of the acoustoelastic constant,

$$2K \Delta \sigma = \left[\frac{\Delta E}{E} - \left(\frac{\epsilon_x}{\nu} - 2\epsilon_x \right) \right] \quad (70)$$

Solving this equation in terms of the change in Young's modulus yields

$$\Delta E = E \times \left[2K \Delta \sigma + \left(\frac{\epsilon_x}{\nu} - 2\epsilon_x \right) \right] \quad (71)$$

This equation expresses the change in elasticity in terms of stress, strain, acoustoelastic constant, and zero stress elasticity. The following table shows how Young's modulus changes as the stress changes.

When using the results presented in this table to compare the elastic change in the direction of the loading with the direction perpendicular the loading be sure to use equal strains not equal stresses.

Table 22: Nonlinearity of Young's Modulus with Strain

Uniaxial Stress (MPa)	Parallel Strain ($\times 10^{-3}$)	Perpendicular Strain ($\times 10^{-3}$)	Parallel ΔE(MPa)	Perpendicular ΔE(MPa)
30	0.45	-0.16	-154	28
61	0.91	-0.31	-308	57
92	1.36	-0.47	-462	85
123	1.81	-0.63	-616	113
153	2.27	-0.78	-770	141
184	2.72	-0.94	-924	170
214	3.17	-1.09	-1077	198
245	3.63	-1.25	-1232	226
276	4.08	-1.41	-1386	254
306	4.53	-1.56	-1540	282
337	4.99	-1.72	-1690	311
368	5.44	-1.88	-1850	340
398	5.89	-2.03	-2000	368
429	6.35	-2.19	-2155	396

REFERENCES

- [1] ACHENBACH, J. D., *Wave propagation in elastic solids*. Elsevier Science Publishers B. V., 1975.
- [2] ASHBY, M. F. and JONES, D. R., *Engineering materials 1*.
- [3] BAZANT, M. Z., *Interatomic Forces in Covalent Solids*. Phd dissertation, Massachusetts Institute of Technology, 1997.
- [4] BERGMAN, R. H. and SHAHBENDER, R. A., “Effects of statically applied stresses on the velocity of propagation of ultrasonic waves,” *Applied Physics*, vol. 29, 1958.
- [5] BERRUTI, T., GOLA, M. M., and BRIGGS, G. D., “Acoustoelastic measurements on aluminium alloy by means of a contact and a non-contact (LFB acoustic microscopy) technique,” *Acoustic Society of America*, vol. 103, pp. 1370–1376, mar 1998.
- [6] DEQUENNOY, M., OUAFTOUH, M., OURAK, M., and JENOT, F., “Theoretical determination of Rayleigh wave acoustoelastic coefficients: comparison with experimental values,” *Ultrasonics*, vol. 39, 2002.
- [7] DORFI, H. R., BUSBY, H. R., and JANSSEN, M., “Acoustoelasticity: Ultrasonic stress field reconstruction,” *Experimental Mechanics*, vol. 36, pp. 325–332, dec 1996.
- [8] DORFI, H. R., BUSBY, H. R., and JANSSEN, M., “Ultrasonic stress measurements based on the generalized acoustic ratio technique,” *International Journal of Solids and Structures*, vol. 33, no. 8, pp. 1157–1174, 1996.
- [9] DOWLING, N. E., *Mechanical behavior of materials*. Prentice-Hall, Inc, 1999.
- [10] DUQUENNOY, M., OUAFTOUH, M., OURAK, M., JENOT, F., and XU, W. J., “Theoretical and experimental determination of the natural and initial acoustoelastic coefficients,” *Review of Quantitative Nondestructive Evaluation*, vol. 21, 2002.
- [11] GRANATO, A. and LUCKE, K., “Theory of mechanical damping due to dislocations,” *Applied Physics*, vol. 27, 1956.
- [12] HSU, N. H., “Acoustic birefringence and use of ultrasonic waves for experimental stress analysis,” *Experimental Mechanics*, vol. 14, no. 5, pp. 169–179, 1974.
- [13] HUGHES, D. S. and KELLY, J. L., “Second-order elastic deformation of solids,” *Physical Review*, vol. 92, pp. 1145–1149, june 1953.
- [14] KENDERIAN, S., BERNT, T. P., GREEN, R. E., and DJORDJEVIC, B. B., “Ultrasonic monitoring of dislocation during fatigue of pearlitic rail steel,” *Material Science and Engineering*, vol. 348, pp. 90–99, june 2003.
- [15] KOBAYASHI, S., “Stress measurement by use of raleigh waves,” *Elsevier Applied Science*, vol. 2, 1992.

- [16] LEE, Y. C. and KUO, S. H., “A new point contact surface acoustic wave transducer for measurement of acoustoelastic effect of polymethylmethacrylate,” *IEEE Transaction on ultrasonics, ferroelectrics, and frequency control*, vol. 51, pp. 114–120, jan 2004.
- [17] MI, B., MICHAELS, T. E., and MICHAELS, J. E., “Ultrasonic techniques for in-situ diagnosis of fatigue crack initiation and growth.” Tentative Publication, Aug. 2005.
- [18] MIN, X. H. and KATO, H., “Change in ultrasonic parameters with loading/unloading process in cyclic loading of aluminium alloy,” *Material Science and Engineering*, vol. 372, pp. 269–277, jan 2004. Min and Kato article.
- [19] QU, J. and LIU, G., “Effects of residual stress on guided waves in layered media,” *Review of Progress in Quantitative Nondestructive Evaluation*, vol. 17, pp. 1635–1642, 1998.
- [20] THURSTON, R. N. and BRUGGER, K., “Third-order elastic constants and velocity of small amplitude elastic waves in homogeneously stressed media,” *Physical Review*, vol. 133, pp. 1604–1149, oct 1963.
- [21] TOUPIN, R. A. and BERSTEIN, B., “Sound waves in deformed perfectly elastic materials. acoustoelastic effect,” *Acoustic Society of America*, vol. 33, 1961.
- [22] UNIVERSITY LIVERPOOL, “Alu-matter.” Internet, <http://aluminium.matter.org.uk>, 2001.